# Engineering the Leap to Inertial Warp Drives

Ioannis Xydous [1]

[1] *BSc. E. Engineering, Piraeus, Greece, E-mail: ioannisxydous@gmail.com*

The longstanding dismissal of inertial propulsion as a violation of Newton's third law is reexamined through a fresh lens. We show that the paradox stems not from any breach of conservation laws, but from a conventional and incomplete application of momentum conservation—one that assumes rigid-body dynamics and overlooks internal force geometry. By analyzing systems with cyclic, non-collinear internal components, we demonstrate that center-of-mass translation can arise without external interaction, via self-contained momentum exchange. This motion emerges directly from Newtonian mechanics, reframing so-called "reactionless" drives as physically valid, self-contained propulsion systems. This reinterpretation resolves the inertial drive paradox and casts decades of anomalous experimental reports not as violations of physics, but as glimpses of an overlooked mechanism. Building on this foundation, we outline a continuum of propulsion architectures: from mechanical constructs to electromagnetic analogs, and ultimately to inertial warp drives. The proposed framework suggests that faster-than-light concepts like the Alcubierre drive may be reimagined—not by bending spacetime, but by bending a system's inertial response. Realization of such systems could redefine spaceship engineering, expanding both the conceptual and technological boundaries of propulsion science.

DOI 10.5281/zenodo.17723628

## I. INTRODUCTION

Among the most enduring frontiers of physics and aerospace engineering is the pursuit of propulsion without expelling reaction mass. More than a theoretical curiosity, this challenge serves as both a stringent test of classical mechanics and a potential gateway to transformative spaceflight technologies. Too often mischaracterized as the quest for "reactionless" drives, the true objective is a *self-contained* propulsion mechanism—one that produces thrust via internal momentum exchange, consistent with conservation laws. Classical mechanics has long deemed such systems impossible, asserting that internal forces cannot accelerate the center of mass of an isolated system [1]. This view has become dominant, leading most claims of inertial propulsion to be dismissed as violations of Newton's third law, regardless of reported evidence. Yet history reveals a recurring pattern. In the mid-20th century, Norman Dean introduced his "Dean Drive," claiming thrust from asymmetrically oscillating masses [4], while V. N. Tolchin developed the "Tolchin Inertoid," a mechanical inertial drive based on rotating masses [5]. Across mechanical [4, 5, 20], electromagnetic [19], and electro-mechanical [16] approaches, the same cycle repeats: anomalous thrust claims spark interest, attract skepticism, and are ultimately attributed to experimental error, thermal effects, or overlooked interactions [6, 9, 14–19, 21]. This persistence suggests not isolated mistakes, but a deeper tension between theory and experiment. This paper challenges the assumption that such anomalies must be illusory. We argue that their rejection stems less from empirical weakness than from a conceptual conflation: *reactionless* propulsion, which is indeed forbidden, has been equated with *self-contained* propulsion, which is not. We show that a system with variable internal configurations can achieve sustained translation by cyclically redistributing its internal masses, allowing net acceleration without external interaction [11]. Broader theoretical connections reinforce this view. Y. N. Ivanov's Rhythmodynamics [13] demonstrates how moving standing waves can generate translation from cyclic internal processes. We propose that such wave-mediated motion is inherently linked to a reduction in effective inertia—allowing massive systems to respond to non-collinear internal forces in ways previously deemed impossible. This insight opens a reinterpretation of faster-than-light concepts such as the Alcubierre warp drive [7], not as spacetime distortions, but as engineered modulations of inertial response. Warp-like motion emerges from internal dynamics that reshape how a standing wave excitation—coupled to its own trapped energy—interacts with its momentum distribution. We extend this concept through a series of mechanical and electromagnetic analogs, replacing orbiting masses with accelerating standing waves confined within toroidal structures. These include microwave waveguide experiments [17, 18], ferrite-core toroidal coils, and mechanical inertial drives designed to induce a net momentum change of the isolated system as a whole [14, 15]. Each configuration explores how phase modulation and tangential acceleration can yield thrust, inertial shielding, or both. Crucially, we introduce a formal link [6, 10, 12, 22] between electromagnetism, gravity, and inertia through the energy density expression—showing that electromagnetic fields can couple to inertial and gravitational effects in ways consistent with conservation laws and measurable thrust. We further derive a relativistic extension [8] to inertial dynamics, showing that proper-time modulation and energy scaling allow for superluminal velocities without invoking exotic matter or spacetime curvature [2, 3]. This inertial warp drive framework reformulates mass, momentum, and velocity expressions to support continuous acceleration across the light-speed threshold. Applying this model to the energy estimates of the Alcubierre drive reveals orders-of-magnitude reductions in required energy, offering a physically grounded alternative to curvature-based propulsion. Validating such mechanisms would not only reinterpret decades of anomalous experiments, but also establish a new paradigm for spaceship engineering: propulsion liberated from reaction mass, operating with unprecedented efficiency, and expanding the boundaries of the physically and technologically possible.

## II. CENTER OF MASS IN ISOLATED SYSTEMS

Persistent experimental anomalies and longstanding confusion highlight the need for a clearer theoretical foundation. Before introducing equations, we must distinguish physically valid concepts from those that violate fundamental laws.

A *reactionless* drive—one that generates thrust without exchanging momentum—is not physically possible, as it violates both momentum conservation and Newton's third law. A *self-contained* propulsion system, however, remains consistent with these laws by keeping momentum exchange internal. Through cyclic internal motion, such systems can produce net acceleration of the center of mass without ejecting mass. Unlike rigid-body textbook models, these systems rely on internal flexibility and oscillatory dynamics.

*Center of Mass.* A deeper understanding begins with the definition of the center of mass, which governs system-level dynamics. For $N$ discrete particles, the rigid-body center of mass is:

$$\vec{R}_{\text{CM,rigid}}(t) = \frac{1}{M}\sum_{i=1}^{N} m_i\,\vec{r}_i(t), \tag{1}$$

where $M = \sum m_i$ is the total mass, and $\vec{r}_i(t)$ is the position of particle $i$.

Newton's second law applied to the system yields:

$$\sum \vec{F}_{\text{ext}} = M\,\frac{d^2}{dt^2}\big(\vec{R}_{\text{CM,rigid}}(t)\big). \tag{2}$$

For an isolated system:

$$\sum \vec{F}_{\text{ext}} + \sum \vec{F}_{\text{int}} = \vec{0} \Rightarrow M\,\frac{d^2}{dt^2}\big(\vec{R}_{\text{CM,rigid}}(t)\big) = \vec{0}. \tag{3}$$

This formulation assumes $\vec{R}_{\text{angular}}(t) = \vec{0}$, meaning all internal forces are pairwise and aligned, with no net angular momentum exchange. Under such constraints, propulsion appears impossible.

However, this limitation applies only to systems with fixed mass distributions and strictly linear internal motion. In systems with cyclic internal changes—such as oscillating or rotating components—the terms in Eq. (1) evolve more dynamically. While total momentum remains conserved, the shifting mass distribution alters the instantaneous center of mass and enables net movement of subsystems.

To describe this behavior more completely, we separate the center of mass into linear and angular components:

$$\vec{R}_{\text{CM}}(t) = \vec{R}_{\text{linear}}(t) + \vec{R}_{\text{angular}}(t). \tag{4}$$

Consider an isolated system (FIG. 1) of $N$ particles: the first $k$ remain stationary, and the remaining $N-k$ form two counter-rotating groups in the $x$–$y$ plane. Let $\vec{r}_{\text{CW}}(t)$ and $\vec{r}_{\text{CCW}}(t)$ denote their positions. If both groups are symmetric and equal in mass, their average positions coincide.

Define:

$$M_{\text{SC}} = \sum_{i=1}^{k} m_i, \quad m_1 = \sum_{i=k+1}^{N_1} m_i, \quad m_2 = \sum_{i=N_1+1}^{N} m_i, \tag{5}$$

$$m_1 = m_2 \equiv m, \quad M_{\text{SC}} = M - 2m. \tag{6}$$

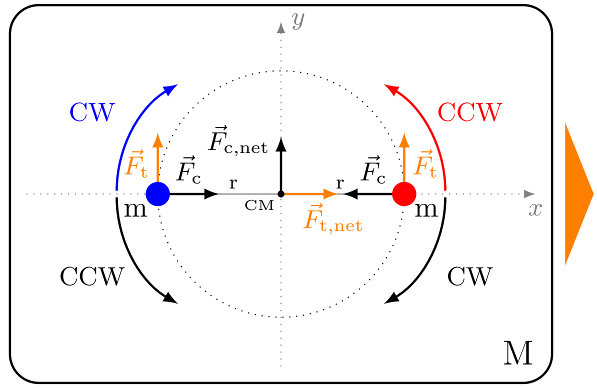


FIG. 1. **Isolated System.** Two counter-rotating masses induce no net torque on the residual mass ($M-2m$). Projected angular contributions yield net tangential thrust (orange arrow) along $x$ and net centripetal force along $y$. Internal linear forces cancel due to symmetry.

Let $\vec{r}_0(t)$ be a fixed inertial reference. Each particle's position is defined relative to this anchor:

$$\vec{r}_i(t) = \vec{r}_0(t) + \begin{pmatrix} x_i + r_i\cos(\theta_i(t)) \\ y_i + r_i\sin(\theta_i(t)) \\ z_i \end{pmatrix}. \tag{7}$$

The total center-of-mass position is:

$$\vec{R}_{\text{CM}}(t) = \frac{1}{M}\sum_{i=1}^{N} m_i\vec{r}_i(t), \tag{8}$$

where $M = \sum m_i$ and $\vec{r}_i(t)$ is the position of particle $i$.

Each particle's position is decomposed into a static offset and a time-dependent angular component:

$$\vec{r}_i(t) = \vec{r}_0(t) + \begin{pmatrix} x_i + r_i\cos(\theta_i(t)) \\ y_i + r_i\sin(\theta_i(t)) \\ z_i \end{pmatrix}, \tag{9}$$

where $\theta_i(t)$ is the angular phase of particle $i$ relative to the inertial reference.

To describe the rotating masses, we define their positions relative to $\vec{r}_0(t)$ using angular displacements. For clockwise and counterclockwise groups:

$$\vec{r}_{\text{CW}}(t) = \frac{1}{M}\sum_{i=k+1}^{N_1} m_i \left[\vec{r}_0(t) + \begin{pmatrix} x_i + r_i\cos(\pi-\omega(t)t) \\ y_i + r_i\sin(\pi-\omega(t)t) \\ z_i \end{pmatrix}\right],$$

$$\vec{r}_{\text{CCW}}(t) = \frac{1}{M}\sum_{i=N_1+1}^{N} m_i \left[\vec{r}_0(t) + \begin{pmatrix} x_i + r_i\cos(\omega(t)t) \\ y_i + r_i\sin(\omega(t)t) \\ z_i \end{pmatrix}\right].$$

To encode zero net torque via symmetry, we define the static group analogously. A phase shift of $\pi$ ensures equal magnitude and opposite direction:

$$\vec{r}_{\mathrm{SC,CW}}(t) = \frac{1}{M}\sum_{i=1}^{j} m_i \left[\vec{r}_0(t) + \begin{pmatrix} x_i + r_i\cos(\omega_{\mathrm{SC}}(t)t) \\ y_i + r_i\sin(\omega_{\mathrm{SC}}(t)t) \\ z_i \end{pmatrix}\right],$$

$$\vec{r}_{\mathrm{SC,CCW}}(t) = \frac{1}{M}\sum_{i=j+1}^{k} m_i \left[\vec{r}_0(t) + \begin{pmatrix} x_i + r_i\cos(\pi + \omega_{\mathrm{SC}}(t)t) \\ y_i + r_i\sin(\pi + \omega_{\mathrm{SC}}(t)t) \\ z_i \end{pmatrix}\right].$$

To simplify subsequent differentiation, we replace $\omega(t)t$ with the phase functions $\phi(t)$ and $\phi_{\mathrm{SC}}(t)$:

$$\vec{r}_{\mathrm{CW}}(t) = \frac{1}{M}\sum_{i=k+1}^{N_1} m_i \left[\vec{r}_0(t) + \begin{pmatrix} x_i + r_i\cos(\pi - \phi(t)) \\ y_i + r_i\sin(\pi - \phi(t)) \\ z_i \end{pmatrix}\right],$$

$$\vec{r}_{\mathrm{CCW}}(t) = \frac{1}{M}\sum_{i=N_1+1}^{N} m_i \left[\vec{r}_0(t) + \begin{pmatrix} x_i + r_i\cos(\phi(t)) \\ y_i + r_i\sin(\phi(t)) \\ z_i \end{pmatrix}\right],$$

$$\vec{r}_{\mathrm{SC,CW}}(t) = \frac{1}{M}\sum_{i=1}^{j} m_i \left[\vec{r}_0(t) + \begin{pmatrix} x_i + r_i\cos(\phi_{\mathrm{SC}}(t)) \\ y_i + r_i\sin(\phi_{\mathrm{SC}}(t)) \\ z_i \end{pmatrix}\right],$$

$$\vec{r}_{\mathrm{SC,CCW}}(t) = \frac{1}{M}\sum_{i=j+1}^{k} m_i \left[\vec{r}_0(t) + \begin{pmatrix} x_i + r_i\cos(\phi_{\mathrm{SC}}(t) + \pi) \\ y_i + r_i\sin(\phi_{\mathrm{SC}}(t) + \pi) \\ z_i \end{pmatrix}\right].$$

The total center-of-mass position is:

$$\vec{R}_{\mathrm{CM}}(t) = \vec{r}_{\mathrm{SC,CW}}(t) + \vec{r}_{\mathrm{SC,CCW}}(t) + \vec{r}_{\mathrm{CW}}(t) + \vec{r}_{\mathrm{CCW}}(t). \tag{10}$$

We now decompose each group into linear and angular components relative to $\vec{r}_0(t)$. Thus,

$$\begin{aligned}\vec{r}_{\mathrm{CW}}(t) = {} & \frac{1}{M}\sum_{i=k+1}^{N_1} m_i \left[\vec{r}_0(t) + \begin{pmatrix} x_i \\ y_i \\ z_i \end{pmatrix}\right] \\ & + \frac{1}{M}\sum_{i=k+1}^{N_1} m_i \begin{pmatrix} r_i\cos(\pi - \phi(t)) \\ r_i\sin(\pi - \phi(t)) \\ 0 \end{pmatrix}. \end{aligned} \tag{11}$$

Under symmetry, both rotating groups share the same average position $\vec{r}(t)$:

$$\sum m_i\vec{r}(t) = m\vec{r}(t). \tag{12}$$

Similarly, the static group's contribution is:

$$\sum m_i\vec{r}_{\mathrm{SC}}(t) = (M - 2m)\vec{r}_{\mathrm{SC}}(t). \tag{13}$$

Assuming uniform radial distances ($r_i = r$ and $r_{\mathrm{SC}}$), angular summations simplify:

$$\sum_{\mathrm{CW}} m_i\vec{r}_i(t) = m\begin{pmatrix} r\cos(\pi - \phi(t)) \\ r\sin(\pi - \phi(t)) \\ 0 \end{pmatrix}, \tag{14}$$

$$\sum_{\mathrm{CCW}} m_i\vec{r}_i(t) = m\begin{pmatrix} r\cos(\phi(t)) \\ r\sin(\phi(t)) \\ 0 \end{pmatrix}. \tag{15}$$

Substituting into group definitions:

$$\vec{r}_{\mathrm{CW}}(t) = \frac{m}{M}\vec{r}(t) + \frac{mr}{M}\begin{pmatrix} \cos(\pi - \phi(t)) \\ \sin(\pi - \phi(t)) \\ 0 \end{pmatrix}, \tag{16}$$

$$\vec{r}_{\mathrm{CCW}}(t) = \frac{m}{M}\vec{r}(t) + \frac{mr}{M}\begin{pmatrix} \cos(\phi(t)) \\ \sin(\phi(t)) \\ 0 \end{pmatrix}. \tag{17}$$

*Inertial Action–Reaction Principle.* Summing position vectors before differentiation conflates geometric symmetry with dynamic behavior. The net force arises from the second derivatives of individual trajectories—spatial cancellation does not imply acceleration cancellation. Forces must be computed from separately differentiated paths.

Using trigonometric identities:

$$\cos(\pi \pm \theta) = -\cos(\theta), \tag{18}$$

$$\sin(\pi - \theta) = \sin(\theta), \quad \sin(\pi + \theta) = -\sin(\theta), \tag{19}$$

we differentiate each component.

Clockwise group:

$$\begin{aligned}\frac{d^2}{dt^2}\vec{r}_{\mathrm{CW}}(t) = {} & \frac{m}{M}\frac{d^2}{dt^2}\vec{r}(t) \\ & + \frac{mr}{M}\left[-\left(\frac{d\phi}{dt}\right)^2\begin{pmatrix} -\cos(\phi(t)) \\ \sin(\phi(t)) \\ 0 \end{pmatrix} + \frac{d^2\phi}{dt^2}\begin{pmatrix} -\sin(\phi(t)) \\ -\cos(\phi(t)) \\ 0 \end{pmatrix}\right],\end{aligned}$$

Counterclockwise group:

$$\begin{aligned}\frac{d^2}{dt^2}\vec{r}_{\mathrm{CCW}}(t) = {} & \frac{m}{M}\frac{d^2}{dt^2}\vec{r}(t) \\ & + \frac{mr}{M}\left[-\left(\frac{d\phi}{dt}\right)^2\begin{pmatrix} \cos(\phi(t)) \\ \sin(\phi(t)) \\ 0 \end{pmatrix} + \frac{d^2\phi}{dt^2}\begin{pmatrix} -\sin(\phi(t)) \\ \cos(\phi(t)) \\ 0 \end{pmatrix}\right],\end{aligned}$$

Residual clockwise:

$$\begin{aligned}\frac{d^2}{dt^2}\vec{r}_{\mathrm{SC,CW}}(t) = {} & \left(\frac{M - 2m}{2M}\right)\frac{d^2}{dt^2}\vec{r}_{\mathrm{SC}}(t) \\ & + \left(\frac{(M - 2m)r_{\mathrm{SC}}}{2M}\right)\left\{\begin{matrix} -\left(\frac{d\phi_{\mathrm{SC}}}{dt}\right)^2\begin{pmatrix} \cos(\phi_{\mathrm{SC}}(t)) \\ \sin(\phi_{\mathrm{SC}}(t)) \\ 0 \end{pmatrix} \\ +\frac{d^2\phi_{\mathrm{SC}}}{dt^2}\begin{pmatrix} -\sin(\phi_{\mathrm{SC}}(t)) \\ \cos(\phi_{\mathrm{SC}}(t)) \\ 0 \end{pmatrix} \end{matrix}\right\},\end{aligned}$$

Residual counterclockwise:

$$\begin{aligned}\frac{d^2}{dt^2}\vec{r}_{\mathrm{SC,CCW}}(t) = {} & \left(\frac{M - 2m}{2M}\right)\frac{d^2}{dt^2}\vec{r}_{\mathrm{SC}}(t) \\ & + \left(\frac{(M - 2m)r_{\mathrm{SC}}}{2M}\right)\left\{\begin{matrix} -\left(\frac{d\phi_{\mathrm{SC}}}{dt}\right)^2\begin{pmatrix} -\cos(\phi_{\mathrm{SC}}(t)) \\ -\sin(\phi_{\mathrm{SC}}(t)) \\ 0 \end{pmatrix} \\ +\frac{d^2\phi_{\mathrm{SC}}}{dt^2}\begin{pmatrix} \sin(\phi_{\mathrm{SC}}(t)) \\ -\cos(\phi_{\mathrm{SC}}(t)) \\ 0 \end{pmatrix} \end{matrix}\right\},\end{aligned}$$

The center-of-mass acceleration decomposes into linear and angular inertial components:

$$M\frac{d^2}{dt^2}\vec{R}_{\rm CM}(t) = M\frac{d^2}{dt^2}\vec{R}_{\rm linear}(t) + M\frac{d^2}{dt^2}\vec{R}_{\rm angular}(t). \tag{20}$$

Linear contribution:

$$M\frac{d^2}{dt^2}\vec{R}_{\rm linear}(t) = (M-2m)\frac{d^2}{dt^2}\vec{r}_{\rm SC}(t) + 2m\frac{d^2}{dt^2}\vec{r}(t). \tag{21}$$

Angular inertial reaction from the residual system vanishes:

$$\vec{F}_{\rm reaction,angular} = \vec{0}. \tag{22}$$

Angular inertial contribution from the rotating masses:

$$\begin{aligned} M\frac{d^2}{dt^2}\vec{R}_{\rm 2m,angular}(t) &= -2mr\left(\frac{d\phi}{dt}\right)^2\begin{pmatrix}0\\ \sin(\phi(t))\\ 0\end{pmatrix} \\ &\quad - 2mr\frac{d^2\phi}{dt^2}\begin{pmatrix}\sin(\phi(t))\\ 0\\ 0\end{pmatrix} \quad (23)\\ &= \vec{F}_{\rm action,angular}. \quad (24)\end{aligned}$$

Although each rotating mass experiences both centripetal and tangential acceleration, the net inertial reaction on the residual system $(M-2m)$ emerges from symmetry. Phase opposition and mass balance yield a composite acceleration vector with tangential ($x$-axis) and centripetal ($y$-axis) components. These are not isolated forces but directional projections of the net inertial response.

Combining all inertial forces contributions:

$$\begin{aligned} M\frac{d^2}{dt^2}\vec{R}_{\rm CM}(t) &= \vec{F}_{\rm reaction,linear} + \vec{F}_{\rm action,linear} \\ &\quad + \vec{F}_{\rm reaction,angular} + \vec{F}_{\rm action,angular}. \end{aligned} \tag{25}$$

Due to symmetry:

$$\vec{F}_{\rm reaction,angular} = \vec{0}, \tag{26}$$

$$\vec{F}_{\rm reaction,linear} + \vec{F}_{\rm action,linear} = \vec{0}. \tag{27}$$

Thus, the net inertial response reduces to:

$$M\frac{d^2}{dt^2}\vec{R}_{\rm CM}(t) = \vec{F}_{\rm action,angular}. \tag{28}$$

*Thrust and Oscillation Components.* This confirms that the center-of-mass acceleration is governed solely by the time-dependent angular displacement of the oscillating masses. Specifically,

$$\sum \vec{F}_{\rm int,angular} \neq \vec{0}, \tag{29}$$

$$M\frac{d^2}{dt^2}\vec{R}_{\rm CM}(t) = \vec{F}_{\rm c,net}(t) + \vec{F}_{\rm t,net}(t) \tag{30}$$

$$\begin{aligned} &= -2mr\left(\frac{d\phi}{dt}\right)^2\begin{pmatrix}0\\ \sin(\phi(t))\\ 0\end{pmatrix} \\ &\quad - 2mr\frac{d^2\phi}{dt^2}\begin{pmatrix}\sin(\phi(t))\\ 0\\ 0\end{pmatrix}. \end{aligned} \tag{31}$$

While Eq. (31) formally accounts for the net thrust $\vec{F}_{\rm t,net}(t)$ arising from internal tangential acceleration, the result remains counterintuitive. It is essential to distinguish this thrust from the internal net centripetal force $\vec{F}_{\rm c,net}(t)$, which governs oscillatory dynamics and results in bound motion without net displacement. A more physically transparent justification will follow in the next section.

Depending on internal constraints, the bulk motion of orbiting mass elements $m$ may follow one of these trajectories:

$$\vec{r}(t) = [r\cos(\omega(t)t),\ r\sin(\omega(t)t),\ 0], \tag{32}$$

$$\vec{r}(t) = [a\cos(\omega(t)t),\ b\sin(\omega(t)t),\ 0], \tag{33}$$

$$\vec{r}(t) = [r\cos(\omega(t)t),\ r\sin(\omega(t)t),\ u_z t], \tag{34}$$

corresponding to circular, elliptical, and helical motion. Each form characterizes the geometry and dynamics of the orbiting structure and may be used to analyze collective inertial effects.

*Energy Balance and Thrust Efficiency.* In an isolated propulsion system, the total mass $M$ includes not only the actuated masses $m$, but also all auxiliary subsystems—power units, motors, supports, and control electronics. Assuming negligible losses, energy conservation requires that any reduction in stored energy matches an increase in mechanical energy.

During a half-cycle, electrical energy is converted into rotational energy and mechanical work:

$$t \in [0, T/2], \tag{35}$$

$$\Delta E^{\rm (electrical)}_{\rm stored} = -\Delta E^{\rm (system)}_{\rm kinetic} = W_{\rm thrust}. \tag{36}$$

If stored electrically (e.g., in a capacitor bank), depletion is:

$$\Delta E^{\rm (electrical)}_{\rm stored} = \frac{1}{2}C\left(V_0^2 - V_c(t)^2\right), \tag{37}$$

where $C$ is capacitance, $V_0$ the initial voltage, and $V_c(t)$ the voltage at time $t$.

The system's kinetic energy change arises from rotational variation:

$$\Delta E^{\rm (system)}_{\rm kinetic} = \sum_{i=1}^{2}\left(\frac{1}{2}I_i\left[\omega(t)^2 - \omega_0^2\right]\right), \tag{38}$$

with $I_i$ the moment of inertia of each rotating mass. For symmetric configurations ($I_1 = I_2 = I$):

$$\Delta E^{\rm (system)}_{\rm kinetic} = I\left[\omega(t)^2 - \omega_0^2\right]. \tag{39}$$

Instantaneous rotational energy:

$$E_{\rm rot}(t) = I\omega(t)^2. \tag{40}$$

Mechanical work from tangential force over the half-cycle:

$$W_{\rm thrust} = \int_0^{T/2} F_{\rm t,net}(t)\cdot u_t(t)\,dt, \tag{41}$$

where $u_t(t)$ is the tangential velocity.

Centripetal force performs no work:

$$W_c = \int_0^{T/2} F_{\rm c,net}(t)\cdot u_c(t)\,dt = 0. \tag{42}$$

Total energy input:

$$E_{\text{total}} = I\omega_0^2 + W_{\text{thrust}}. \tag{43}$$

Thrust efficiency:

$$\eta_t = \frac{W_{\text{thrust}}}{E_{\text{total}}}. \tag{44}$$

This formulation accounts for both passive rotational energy and active tangential work, yielding a closed and physically consistent energy budget under idealized conditions.

## III. INERTIA-DRIVEN TRANSLATION MECHANISM

As shown in Eq. (31), the center of mass can be propelled by internal angular forces. To an external observer unaware of internal dynamics, such motion appears paradoxical. This suggests that a time-varying distribution of inertia may enable self-propulsion through purely internal means.

Since the center of mass combines linear and angular components, its acceleration arises from internal momentum redistribution—particularly via time-dependent angular modulation. Although the system is closed and free from external forces, its internal degrees of freedom dynamically reshape the effective inertia, allowing net acceleration without violating conservation laws.

Mathematically, we consider the total time derivative of the system's linear momentum:

$$\frac{d\vec{P}}{dt} = \frac{dM}{dt} \cdot \vec{V}_{\text{R}}(t) + M(t) \cdot \frac{d\vec{V}_{\text{CM}}}{dt}. \tag{45}$$

In the absence of external forces:

$$\frac{d\vec{P}}{dt} = \vec{0}, \tag{46}$$

unless the system undergoes internal reconfiguration. If $\frac{d\vec{P}}{dt} \neq 0$, the momentum change must be sourced internally. For a variable-mass system:

$$\vec{F}_{\text{t,net}}(t) = \vec{F}_{\text{thrust}}(t) = \frac{d\vec{P}}{dt} = \frac{dM}{dt} \cdot \vec{V}_{\text{R}}(t), \tag{47}$$

where $\vec{V}_{\text{R}}(t)$ is the velocity of exchanged mass relative to the system.

By analogy with the rocket equation, we assume $\vec{V}_{\text{R}}$ is constant, while $M(t)$—interpreted as time-varying inertia—decreases due to evolving internal angular dynamics. Setting $V_{\text{R}} = V_{\max}$, Eq. (47) simplifies to:

$$F_{\text{thrust}}(t) = \frac{dP}{dt} = -\frac{dM}{dt} \cdot V_{\max}, \qquad \text{with} \quad \frac{dM}{dt} < 0, \tag{48}$$

where the negative rate $\frac{dM}{dt}$ reflects inertia reduction via internal reconfiguration.

Rewriting Eq. (48):

$$dM \cdot V_{\max} = -F_{\text{thrust}}(t) \cdot dt, \tag{49}$$

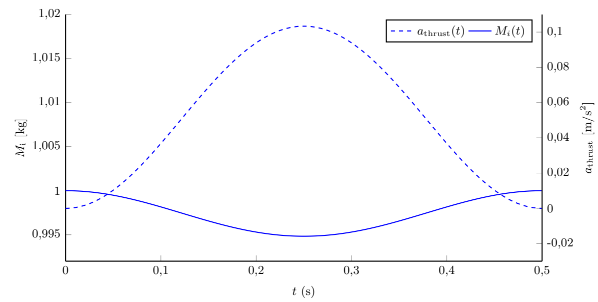


FIG. 2. **Effective Inertia.** Time-resolved simulation of $M_{\text{i}}(t)$ under thrust modulation. Left axis: inertia reduction. Right axis: thrust acceleration. Parameters: $f = 1\,\text{Hz}$, $T = 1\,\text{s}$, $a_{\max} = 2\,\text{m/s}^2$, $\phi_0 = \frac{\pi}{6}$, $M = 1\,\text{kg}$, $m = 0.05\,\text{kg}$, $r = 0.1\,\text{m}$.

and integrating over $t \in [t_1, t_2]$ with $T/2 = t_2 - t_1$:

$$V_{\max} \cdot (M_i - M) = -\int_{t_1}^{t_2} F_{\text{thrust}}(t)dt, \tag{50}$$

where $M_i$ is the effective inertia after time $T/2$ and $M$ is the initial value.

To ensure consistent interpretation, we define thrust as a positive scalar:

$$F_{\text{t,net}}(t) = F_{\text{thrust}}(t) = 2m\,|a_{\text{thrust}}(t)|\,, \tag{51}$$

where $a_{\text{thrust}}(t)$ is the instantaneous tangential acceleration. This avoids sign ambiguity and ensures $M_i < M$ during propulsion (see FIG. 2).

Substituting into Eq. (50):

$$M_i = M - \frac{2m}{V_{\max}} \int_{t_1}^{t_2} |a_{\text{thrust}}(t)| \cdot dt. \tag{52}$$

For symmetric excitation over $[0, T/2]$, we approximate:

$$\int_0^{T/2} |a_{\text{thrust}}(t)|\ dt \approx |a_{\text{thrust}}(t)| \cdot \frac{T}{2}. \tag{53}$$

Defining maximum acceleration:

$$a_{\max} := \frac{V_{\max}}{T/2}, \tag{54}$$

we obtain a pointwise estimate:

$$M_i(t) \approx M - \frac{2m}{a_{\max}} \cdot |a_{\text{thrust}}(t)|\,. \tag{55}$$

This diagnostic formulation estimates inertia reduction from the instantaneous thrust profile. It is valid when $a_{\text{thrust}}(t)$ is smooth, bounded, and approximately sinusoidal.

## IV. DUAL-OSCILLATOR PROPULSION AS A TRAVELLING–STANDING WAVE SYSTEM

Y. N. Ivanov's 1997 monograph [13], *Rhythmodynamics*, introduces the concept of a *moving standing wave*—a dynamic

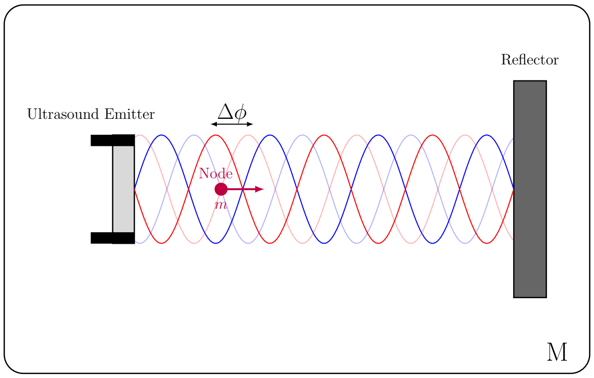


FIG. 3. **Travelling Standing Waves.** Isolated System. Ivanov's theory: two counter-propagating sinusoidal waves form a standing wave—trapping mass $m$ in its node—whose envelope translates. The red arrow labeled *Node* indicates motion along the $x$-axis, while oscillations occur transversely along $y$. Node acceleration arises from time-varying phase modulation. At the system level ($M$), no net acceleration occurs because the internal inertial action–reaction forces cancel under collinearity.

interference pattern whose continuous phase evolution enables self-propulsion. Unlike classical standing waves, Ivanov's formulation exhibits directional compression along the axis of motion, with mass $m$ trapped in the translating node. This behavior, verified through acoustic analogs, reveals a propulsion mechanism based on internal angular modulation, where rhythmic phase shifts generate velocity and acceleration without external force.

*Ivanov's Theory.* Consider two sinusoidal waves of equal amplitude $A$, angular velocity $\omega$, and wave number $k$, propagating in opposite directions along $x$:

$$y_1(x,t) = A\sin(kx - \omega t) \quad \text{(rightward)} \tag{56}$$
$$y_2(x,t) = A\sin(kx + \omega t) \quad \text{(leftward)} \tag{57}$$

Their sum yields:

$$y(x,t) = y_1(x,t) + y_2(x,t) \tag{58}$$
$$= A\sin(kx - \omega t) + A\sin(kx + \omega t). \tag{59}$$

Using the identity:

$$\sin(a-b) + \sin(a+b) = 2\sin(a)\cos(b), \tag{60}$$

we obtain:

$$y(x,t) = 2A\sin(kx)\cos(\omega t). \tag{61}$$

This describes a standing wave with spatial nodes from $\sin(kx)$ and temporal oscillation from $\cos(\omega t)$. Applying a time-dependent spatial phase shift $\phi(t)$:

$$y(x,t) = 2A\sin(kx + \phi(t))\cos(\omega t) \tag{62}$$
$$= A\sin(kx + \phi(t) - \omega t) + A\sin(kx + \phi(t) + \omega t). \tag{63}$$

Nodes occur where:

$$\sin(kx + \phi(t)) = 0 \quad \Rightarrow \quad kx + \phi(t) = n\pi, \tag{64}$$

yielding node position:

$$x_n(t) = \frac{n\pi - \phi(t)}{k}. \tag{65}$$

Differentiating:

$$u_{\text{node}} = \frac{dx_n}{dt} = -\frac{1}{k}\cdot\frac{d\phi}{dt}. \tag{66}$$

The sign of $\frac{d\phi}{dt}$ determines node direction: positive shifts nodes leftward, negative shifts them rightward. This inverse relationship arises from how $\phi(t)$ enters the spatial argument.

In practice, generator control determines whether the phase shift is temporal or spatial. A constant phase offset applied to both signals yields a temporal shift—leaving nodes stationary. To induce node motion, the phase shift must vary with time and enter the spatial argument, typically by modulating one generator relative to the other. This evolving phase difference actively translates the standing wave pattern and forms the basis of dynamic standing wave propulsion.

Node acceleration follows:

$$a_{\text{node}} = \frac{du_{\text{node}}}{dt} = -\frac{1}{k}\cdot\frac{d^2\phi}{dt^2}. \tag{67}$$

The sign of $\frac{d^2\phi}{dt^2}$ governs acceleration direction: positive accelerates nodes leftward, negative accelerates them rightward. The second derivative captures the curvature of phase modulation and serves as a geometric proxy for internal force.

Controlling $\phi(t)$ enables rhythmic acceleration of the wave structure without external force. The curvature of its trajectory encodes the internal momentum exchange that underlies propulsion.

The derivative $\frac{d\phi}{dt}$ represents the instantaneous phase rate. Assuming $\phi(t)$ is smooth and differentiable, it captures phase evolution at infinitesimal scale.

Ivanov approximates this with a finite difference:

$$\frac{d\phi}{dt} \quad \longrightarrow \quad \frac{\Delta\phi}{\Delta t},$$

yielding a discrete formulation consistent with his stepwise phase update method—though notably omitting the negative sign present in the continuous case.

Consequently, taking the finite time steps approach, the node velocity and acceleration become:

$$k = \frac{2\pi}{\lambda}, \quad \Delta t = \frac{T}{2}, \quad \lambda = u_{\max}\cdot T, \tag{68}$$
$$u_{\text{node}} = -\frac{1}{k}\cdot\frac{\Delta\phi}{\Delta t} = -u_{\max}\cdot\frac{\Delta\phi}{\pi}, \tag{69}$$
$$a_{\text{node}} = -\frac{1}{k}\cdot\frac{\Delta^2\phi}{\Delta t^2} = -\frac{1}{k}\cdot\frac{\Delta\omega}{\Delta t} = 2u_{\max}\cdot\Delta f. \tag{70}$$

By setting $u_{\max} = c$ and taking absolute values, we obtain Ivanov's expressions:

$$|u_{\text{node}}| = c\cdot\frac{\Delta\phi}{\pi}, \tag{71}$$
$$|a_{\text{node}}| = 2c\cdot\Delta f. \tag{72}$$

*Imposed Geometric Curvature as a Prerequisite.* Ivanov's rhythmodynamics derives motion from discrete phase and frequency shifts, but never explicitly requires curvature. Our model makes this condition explicit: to generate angular force or torque, the standing wave—or orbiting mass—must follow a curved path. Without curvature, node acceleration remains collinear, producing no net displacement.

This elevates curvature from an implicit effect to a geometric prerequisite, bridging discrete modulation and continuous dynamics. It also enables both mass trapping within standing wave nodes and the use of standing waves as dynamic, massless carriers of inertia—a concept not raised in Ivanov's Rhythmodynamics.

Ivanov's expressions omit explicit time dependence, relying on $\Delta\phi$ and $\Delta f$. To align with our model, we embed the standing wave in circular geometry:

$$y(\phi(t), t) = 2A\sin(kr\phi(t))\cos(\omega t), \tag{73}$$

where $kr\phi(t)$ tracks arc length. In contrast:

$$y(\phi(t), t) = 2A\sin(kr + \phi(t))\cos(\omega t), \tag{74}$$

is structurally similar to the linear form:

$$y(x, t) = 2A\sin(kx + \phi(t))\cos(\omega t),$$

where $\phi(t)$ acts as a time-dependent phase offset. This does not embed the wave into circular geometry, as it treats $\phi(t)$ as a shift rather than a coordinate.

To reflect angular displacement, the wave must be expressed as $\sin(kr\phi(t))$.

Transforming to geometric form:

$$y(\phi(t), t) = 2A\sin(kr\phi(t))\cos(\omega t), \tag{75}$$

$$\vec{R}(t) = [r + y(\phi(t), t)]\begin{pmatrix}\cos(\phi(t))\\ \sin(\phi(t))\\ 0\end{pmatrix}. \tag{76}$$

This formulation allows direct computation of velocity and acceleration via time derivatives. The wave's amplitude modulates radial displacement, while angular evolution generates tangential and centripetal force components. All inertial drive dynamics emerge naturally from this embedded structure.

The total acceleration of a standing wave embedded in a circular path is:

$$\begin{aligned}\frac{d^2\vec{R}}{dt^2} &= \left[\frac{d^2y}{dt^2} - (r+y)\left(\frac{d\phi}{dt}\right)^2\right]\begin{pmatrix}\cos(\phi)\\ \sin(\phi)\\ 0\end{pmatrix}\\ &+ 2\cdot\frac{dy}{dt}\cdot\frac{d\phi}{dt}\begin{pmatrix}-\sin(\phi)\\ \cos(\phi)\\ 0\end{pmatrix}\\ &+ (r+y)\cdot\frac{d^2\phi}{dt^2}\begin{pmatrix}-\sin(\phi)\\ \cos(\phi)\\ 0\end{pmatrix}.\end{aligned} \tag{77}$$

In the absence of external forces, the linear acceleration component must vanish:

$$\frac{d^2y}{dt^2} = 0 \quad\Rightarrow\quad \frac{dy}{dt} = 0.$$

Substituting yields:

$$\begin{aligned}\frac{d^2\vec{R}}{dt^2} &= -(r+y)\left(\frac{d\phi}{dt}\right)^2\begin{pmatrix}\cos(\phi)\\ \sin(\phi)\\ 0\end{pmatrix}\\ &+ (r+y)\cdot\frac{d^2\phi}{dt^2}\begin{pmatrix}-\sin(\phi)\\ \cos(\phi)\\ 0\end{pmatrix}.\end{aligned} \tag{78}$$

To align node radius with wave number $k = \frac{2\pi}{\lambda}$, we impose:

$$r + y(\phi(t), t) = \frac{1}{k}. \tag{79}$$

This synchronizes wave modulation with loop geometry, ensuring consistent node placement and symmetric acceleration. It is a design choice—not a derivational necessity—that simplifies analysis.

Tangential acceleration becomes:

$$\vec{a}_{\mathrm{t}} = \frac{1}{k}\cdot\frac{d^2\phi}{dt^2}\begin{pmatrix}-\sin(\phi)\\ \cos(\phi)\\ 0\end{pmatrix}. \tag{80}$$

This illustrates how angular acceleration couples with wave-modulated radius to generate net tangential force.

The function $y(\varphi(t), t)$ may represent a field component or localized energy density. When accelerated—especially via angular variation—it produces inertial force.

Comparing Eq. (31) and Eq. (80), we note the latter includes a $y$-axis contribution. To restore symmetry, we introduce a second standing wave in a nearby plane, rotating oppositely. This yields a CW–CCW pair for inertial coupling and unidirectional thrust.

Position vectors:

$$\vec{R}_{\mathrm{CW}}(t) = [r + y(\phi, t)]\begin{pmatrix}\cos(\pi-\phi)\\ \sin(\pi-\phi)\\ 0\end{pmatrix}, \tag{81}$$

$$\vec{R}_{\mathrm{CCW}}(t) = [r + y(\phi, t)]\begin{pmatrix}\cos(\phi)\\ \sin(\phi)\\ 0\end{pmatrix}. \tag{82}$$

Tangential accelerations:

$$\vec{a}_{\mathrm{t,CW}}(t) = \frac{1}{k}\cdot\frac{d^2\phi}{dt^2}\begin{pmatrix}-\sin(\phi)\\ -\cos(\phi)\\ 0\end{pmatrix}, \tag{83}$$

$$\vec{a}_{\mathrm{t,CCW}}(t) = \frac{1}{k}\cdot\frac{d^2\phi}{dt^2}\begin{pmatrix}-\sin(\phi)\\ \cos(\phi)\\ 0\end{pmatrix}. \tag{84}$$

Summing yields net acceleration:

$$\begin{aligned}\vec{a}_{\mathrm{t,net}}(t) &= \vec{a}_{\mathrm{t,CW}}(t) + \vec{a}_{\mathrm{t,CCW}}(t)\\ &= \frac{1}{k}\cdot\frac{d^2\phi}{dt^2}\begin{pmatrix}-2\sin(\phi)\\ 0\\ 0\end{pmatrix}.\end{aligned} \tag{85}$$

**Important**: The net tangential acceleration of the standing wave pair acts as the trigger for rising thrust, but it does not represent the actual thrust magnitude. The confined electromagnetic energy density ultimately dictates both the thrust force and the resulting acceleration.

## V. MECHANICAL INERTIAL DRIVE

The net internal force in Eq. (31) decomposes into two orthogonal components: a centripetal term $\propto \left(\frac{d\phi}{dt}\right)^2$ and a tangential term $\propto \frac{d^2\phi}{dt^2}$. While both act instantaneously, only the tangential component contributes to net displacement of the center of mass.

Counterintuitively, the tangential force projects along the $x$-axis, while the centripetal force acts along $y$. The centripetal contribution integrates to a bounded excursion and vanishes as $\frac{d\phi}{dt} \to 0$. Any asymmetry in angular velocity is self-restoring: deceleration or cessation generates a centripetal force of opposite sign, halting the system. This arises from the squared velocity dependence, which collapses the radial force as motion ceases.

In contrast, the tangential component governs angular momentum exchange. Its contribution accumulates under angular acceleration, producing a net shift in the center-of-mass velocity and thereby enabling the conversion of rotational energy into linear motion.

Once acceleration ceases, the orbiting masses continue at constant angular velocity, and the system retains its acquired translational speed. Unlike the centripetal term, tangential acceleration breaks time-reversal symmetry and yields unbounded displacement, making it the sole viable mechanism for sustained, propellantless propulsion.

FIG. 4 illustrates the conceptual basis. To enable independent modulation of orbital speeds without interrupting rotation, the two counter-orbiting masses must occupy separate planes. This spatial separation allows dynamic control of angular phase without requiring a full stop.

*Phase Modulation.* To model this behavior, the angular phase is prescribed as:

$$\phi(t) = \phi_0 \cdot \sin\left(\frac{2\pi t}{T}\right), \tag{86}$$

where $\phi_0$ is peak angular displacement and $T$ the cycle period. Angular velocity and acceleration follow:

$$\omega(t) = \frac{d\phi}{dt} = \phi_0 \cdot \frac{2\pi}{T} \cdot \cos\left(\frac{2\pi t}{T}\right), \tag{87}$$

$$\alpha(t) = \frac{d^2\phi}{dt^2} = -\phi_0 \cdot \left(\frac{2\pi}{T}\right)^2 \cdot \sin\left(\frac{2\pi t}{T}\right). \tag{88}$$

FIG. 5 shows the resulting force profiles. The tangential force $F_x(t)$ is rectified and unidirectional; the centripetal force $F_y(t)$ oscillates around zero and is suppressed by a factor of 4.6. Notably, $\omega(t)$ crosses zero, implying reversal in rotation direction. This requires both motors to stop and reverse synchronously—precisely at $t = T/4$, when $F_x(t)$ peaks.

While acceptable in simulation, practical systems require uninterrupted rotation during thrust phases. FIG. 6 introduces a constant angular velocity offset $\omega_{\text{offset}}$, enabling unidirectional motor driving. This offset amplifies $F_y(t)$ and must be tuned to preserve thrust efficiency. Simulations show optimal performance when $F_x(t)$ and $F_y(t)$ amplitudes are matched.

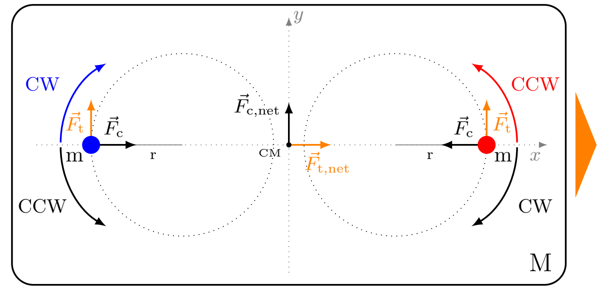


FIG. 4. **Mechanical Inertial Drive.** Two oscillating masses orbit on separate planes within an isolated system. This topology enables independent control of angular velocity. When orbiting speed is constant, the system yields no net thrust. Thrust (orange arrow) arises only during angular acceleration, enabling momentum exchange via controlled phase modulation $\phi$.

FIG. 7 illustrates poor tuning: excessive offset and large $\phi_0$ lead to centripetal dominance and tangential suppression. Historically, such misconfigurations have led to misidentified thrust along $y$—where $F_y(t)$ resides—while overlooking true propulsion along $x$.

This interpretation is based solely on present analysis; no prior diagnostics are known. To quantify motion, we compute the change in linear momentum over one cycle using average thrust $\langle F_{\text{thrust}} \rangle$:

$$\Delta p = \langle F_{\text{thrust}} \rangle \cdot T = 0.0387\,\text{kg} \cdot \text{m/s}. \tag{89}$$

Assuming a total system mass of $M = 1$ kg and no external forces, the final velocity after a $t_{\text{coast}} = 5$ s coasting phase is:

$$u_f = \frac{\Delta p}{M} = 0.0387\,\text{m/s} = 0.1393\,\text{km/h} \tag{90}$$

This velocity remains constant throughout the coasting phase, as no internal or external forces act to alter the system's momentum.

Increasing the base frequency to 5 Hz yields:

$$\Delta p = 0.1938\,\text{kg} \cdot \text{m/s}, \tag{91}$$
$$u_f = 0.1938\,\text{m/s} = 0.6976\,\text{km/h}. \tag{92}$$

Corresponding average thrust:

$$\langle F_{\text{thrust}} \rangle = \frac{\Delta p}{T} = 0.9691\,\text{N}. \tag{93}$$

*Test I.* A configuration operating at $f = 10$ Hz—similar to FIG. 6 but differing in frequency—offers a promising setup for experimental validation. Consider a 1 kg device sliding on a lubricated plastic base. The normal force:

$$F_N = Mg = 1 \cdot 9.81 = 9.81\,\text{N}. \tag{94}$$

Typical friction coefficients:

$$\mu_s = 0.15 \quad \text{(static)}, \tag{95}$$
$$\mu_k = 0.10 \quad \text{(kinetic)}. \tag{96}$$

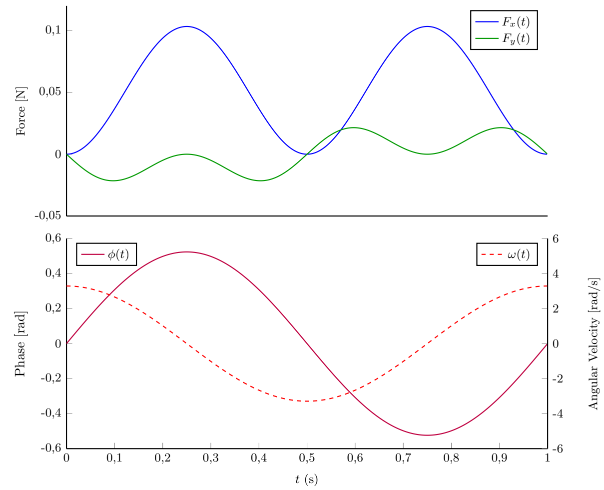


FIG. 5. **Internal Forces and Angular Dynamics.** Time-resolved dynamics over one cycle. Tangential force $F_x(t)$ (top) accumulates net momentum and dominates $F_y(t)$ by a factor of 4.6. Angular phase $\phi(t)$ and velocity $\omega(t)$ (bottom) shown with dual $y$-axes. Sinusoidal phase yields asymmetric acceleration. Parameters: $f = 1\,\text{Hz}$, $T = 1\,\text{s}$, $\phi_0 = \frac{\pi}{6}$, $M = 1\,\text{kg}$, $m = 0.05\,\text{kg}$, $r = 0.1\,\text{m}$.

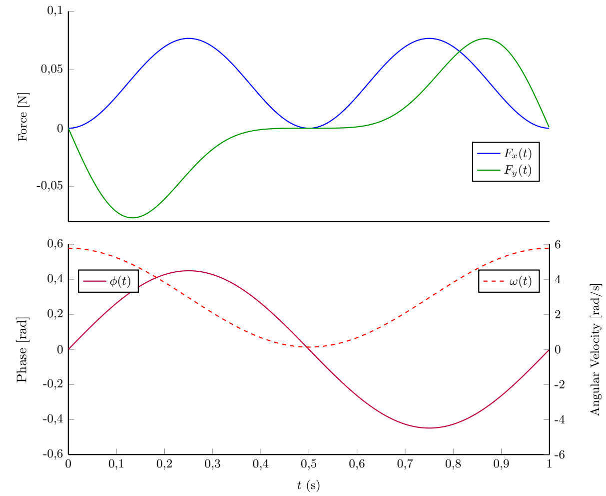


FIG. 6. **Unidirectional Motor Driving and Force Symmetry.** A practical inertial drive using unidirectional motor control. Applying a constant angular velocity offset $\omega_{\text{offset}}$ enhances the centripetal force. To restore thrust symmetry, the offset is tuned so both forces reach equal amplitude. Parameters: $f = 1\,\text{Hz}$, $T = 1\,\text{s}$, $\phi_0 = \frac{\pi}{7}$, $\omega_{\text{offset}} = 0.47 \cdot \omega_0$, $M = 1\,\text{kg}$, $m = 0.05\,\text{kg}$, $r = 0.1\,\text{m}$.

Corresponding friction forces:

$$F_{\text{static}} = \mu_s F_N = 1.4715\,\text{N}, \tag{97}$$

$$F_{\text{kinetic}} = \mu_k F_N = 0.981\,\text{N}. \tag{98}$$

Generated average thrust:

$$\langle F_{\text{thrust}} \rangle = 3.8765\,\text{N}. \tag{99}$$

Since thrust exceeds both friction thresholds, the system initiates forward motion under ideal conditions. The static friction is ∼2.6× weaker than the thrust and is overcome within the first 0.009 s of the cycle. Thereafter, only kinetic friction remains.

Net force overcoming kinetic friction:

$$F_{\text{net}} \approx 3.8765 - 0.981 = 2.8955\,\text{N}. \tag{100}$$

Momentum change over full-cycle $T = 0.1\,\text{s}$:

$$\Delta p = F_{\text{net}} \cdot T = 0.2895\,\text{kg} \cdot \text{m/s}. \tag{101}$$

Final velocity:

$$u_f = \frac{\Delta p}{M} = 0.2895\,\text{m/s} = 1.0422\,\text{km/h}. \tag{102}$$

This velocity remains constant during coasting, confirming sustained translation from internal acceleration.

The average net acceleration per mass is:

$$a_{\text{m}} = \frac{3.8765}{2 \cdot 0.050} = 38.76\,\text{m/s}^2, \tag{103}$$

a substantial value within practical limits. Operating at lower frequencies (1–10 Hz) may reduce this, though achieving low-friction contact remains essential.

*Test II.* Overcoming gravity. Consider the inertial propulsion system operating at $f = 15.91$ Hz, using the parameters of FIG. 6 except for increased frequency. The full-cycle duration is:

$$T = \frac{1}{f} = \frac{1}{15.91} \approx 0.06285\,\text{s}. \tag{104}$$

In this vertical configuration, the net average thrust force is directed upward. From numerical integration:

$$\langle F_{\text{thrust}} \rangle = 9.81\,\text{N}. \tag{105}$$

Gravitational force on the 1 kg device:

$$F_g = Mg = 1 \cdot 9.81 = 9.81\,\text{N}. \tag{106}$$

Net upward force:

$$F_{\text{net}} = \langle F_{\text{thrust}} \rangle - F_g = 0\,\text{N}. \tag{107}$$

Impulse over thrust duration:

$$\Delta p_{\text{up}} = F_{\text{net}} \cdot T = 9.81 \cdot 0.06285 \approx 0.6165\,\text{kg} \cdot \text{m/s}. \tag{108}$$

Assuming the system starts from rest, upward velocity gained:

$$\Delta u_{\text{up}} = \frac{\Delta p_{\text{up}}}{M} = 0.6165\,\text{m/s}. \tag{109}$$

Downward velocity from gravity:

$$\Delta u_{\text{down}} = -g \cdot T = -9.81 \cdot 0.06285 \approx -0.6165\,\text{m/s}. \tag{110}$$

Net velocity change:

$$\Delta u_{\text{cycle}} = \Delta u_{\text{up}} + \Delta u_{\text{down}} = 0\,\text{m/s}. \tag{111}$$

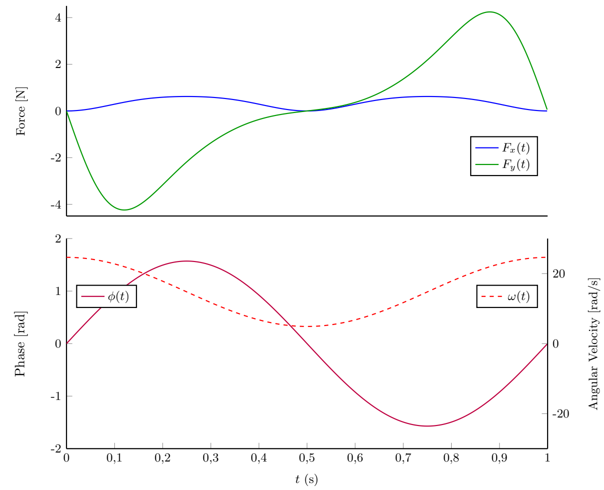


FIG. 7. **Mistuned Inertial Drive.** A large angular velocity offset $\omega_{\text{offset}} = 2.35 \cdot \omega_0$ and high phase amplitude $\phi_0 = \frac{\pi}{2}$ lead to centripetal force domination by a factor of 7.4 and suppression of the tangential component. Parameters: $f = 1\,\text{Hz}$, $T = 1\,\text{s}$, $M = 1\,\text{kg}$, $m = 0.05\,\text{kg}$, $r = 0.1\,\text{m}$.

This indicates dynamic equilibrium: upward thrust impulse cancels gravitational impulse per cycle. The device hovers at fixed altitude without net acceleration. The average acceleration per oscillating mass is:

$$a_{\text{m}} = \frac{9.81}{2 \cdot 0.050} = 98.1\,\text{m/s}^2. \tag{112}$$

This $98.1\,\text{m/s}^2$ acceleration presents a significant engineering challenge—equivalent to $10\,g$, well beyond typical actuator limits.

In contrast, *Test I* remains feasible with conventional techniques, especially at lower frequencies and larger orbital radii. If low-friction constraints are managed, this setup offers a viable path to experimentally validate inertial propulsion.

## VI. ELECTROMAGNETIC INERTIAL DRIVE (MICROWAVE WAVEGUIDES)

The experimental implementation of two counter-propagating standing waves can be realized using a pair of circular microwave waveguides, each driven by magnetron-based generators. The waveguides are terminated to allow reflection at their endpoints, forming closed-loop standing wave patterns (see FIG. 8). A time-varying phase shift is applied symmetrically to each waveguide, enabling controlled rotation of the standing wave.

As previously demonstrated, thrust arises from the net tangential acceleration of the counter-rotating standing waves:

$$\vec{a}_{\text{t,net}}(t) = -\frac{2}{k} \cdot \frac{d^2\phi}{dt^2} \begin{pmatrix} \sin(\phi(t)) \\ 0 \\ 0 \end{pmatrix}. \tag{113}$$

The left waveguide induces clockwise rotation via $\phi_L(t)$; the right induces counterclockwise rotation via $\phi_R(t)$, with

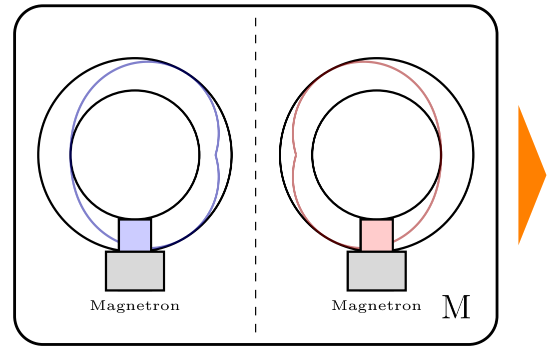


FIG. 8. **Electromagnetic Inertial Drive.** Electromagnetic analog to the mechanical inertial drive, using toroidal waveguides powered by a magnetron via a stub impedance matcher. Reflections at the waveguide ends form standing waves. A time-dependent phase shift modulates these standing waves—shown in blue (CW) and red (CCW)—producing net tangential acceleration (real thrust (orange arrow)) along the $x$-axis, resulting in an induced linear thrust on the system $M$.

$\phi_R(t) = -\phi_L(t)$ to maintain symmetry. This configuration generates net tangential acceleration while preserving angular momentum balance.

The standing wave is geometrically constrained by:

$$r + y(\phi(t), t) = \frac{\lambda_g}{2\pi} = \frac{1}{k_g}, \tag{114}$$

where $r$ is the static waveguide radius, $y(\phi(t), t)$ the radial modulation, $\lambda_g$ the guided wavelength, and $k_g = \frac{2\pi}{\lambda_g}$ the guided wave number. This ensures the wavefront's radial position matches the spatial phase scale of the guided mode.

*Cutoff Frequency.* For the $\text{TE}_{11}$ mode in a toroidal waveguide of radius $r$, the cutoff frequency is:

$$f_c = \frac{x_{11} \cdot c}{2\pi r_c}, \tag{115}$$

where $x_{11} \approx 1.841$ is the first root of $J_1'(x) = 0$, and $c$ is the speed of light. Here, $J_1(x)$ is the Bessel function of the first kind (order one), and $J_1'(x)$ its derivative, which governs cutoff conditions for transverse electric modes. The cutoff frequency is inversely proportional to the cross-sectional radius $r_c$.

*Waveguide Constraints.* To preserve physical validity, the ring radius $r = r_g$—measured from the torus center to the midpoint of its cross section—must satisfy:

$$r = r_g \geq 3r_c. \tag{116}$$

This thin-ring constraint minimizes curvature distortion and suppresses unwanted mode coupling. It also imposes a lower bound on the ratio $f_c/f$, since both $r_c$ and $r_g$ scale inversely with cutoff and operating frequencies. Satisfying this inequality ensures clean azimuthal mode propagation and supports the assumptions of the standing-wave thrust model.

*Guided Wavelength.* Assuming an operating frequency of $f = 2\,\text{GHz}$ and a waveguide filled with air, the guided wavelength is:

$$\lambda_g = \frac{\lambda_0}{\sqrt{1 - \left(\frac{f_c}{f}\right)^2}}, \quad \lambda_0 = \frac{c}{f}. \tag{117}$$

For $r_c = 0.0443$ m, we compute:

$$f_c \approx \frac{1.841 \cdot 3 \cdot 10^8}{2\pi \cdot 0.0443} \approx 1.984\,\text{GHz}, \tag{118}$$

$$\lambda_0 = \frac{3 \cdot 10^8}{1.984 \cdot 10^9} \approx 0.1511\,\text{m}, \tag{119}$$

$$\lambda_g \approx \frac{0.1511}{\sqrt{1 - \left(\frac{1.984}{2}\right)^2}} \approx 1.2055\,\text{m}. \tag{120}$$

*Group Velocity.* The group velocity of the $\text{TE}_{11}$ mode in a toroidal waveguide is:

$$u_g = c \cdot \sqrt{1 - \left(\frac{f_c}{f}\right)^2}, \tag{121}$$

where $c = 3 \cdot 10^8$ m/s is the speed of light, $f = 2$ GHz the operating frequency, and $f_c \approx 1.984$ GHz the cutoff frequency for $r_c = 0.0443$ m. Substituting:

$$u_g \approx 3 \cdot 10^8 \cdot \sqrt{1 - \left(\frac{1.984}{2}\right)^2} \approx 3.7602 \cdot 10^7\,\text{m/s}. \tag{122}$$

Since $f_c < f$, the $\text{TE}_{11}$ mode propagates. To support a full circumferential standing wave with azimuthal mode number $n = 1$, the ring radius must satisfy:

$$r_g = \frac{\lambda_g}{2\pi} \approx \frac{1.2055}{6.283} \approx 0.1918\,\text{m}, \quad \frac{r_g}{r_c} \approx 4.33, \tag{123}$$

ensuring one guided wavelength fits around the ring. The corresponding path length:

$$L = 2\pi r_g \approx 1.2055\,\text{m}. \tag{124}$$

*Energy Density.* The electromagnetic energy density of each standing wave is:

$$w_{\text{EM}}(t) = \frac{1}{2}\varepsilon_0 |\vec{E}(t)|^2 + \frac{1}{2}\frac{|\vec{B}(t)|^2}{\mu_0}, \tag{125}$$

where $\vec{E}(t)$ and $\vec{B}(t)$ are the superposed fields. Since the waves are spatially stationary:

$$w_{\text{EM}}(t) \neq \frac{D_{\text{EM}}(t)}{u_g} \quad \Rightarrow \quad D_{\text{EM}}(t) = 0, \tag{126}$$

where $D_{\text{EM}}(t)$ is the power density and $u_g$ the group velocity.

However, when the envelope moves, power density becomes:

$$D_{\text{EM}}(t) = w_{\text{EM}}(t) \cdot u_{\text{t,net}}(t), \tag{127}$$

with $u_{\text{t,net}}(t)$ the net tangential velocity of the envelope. Taking the time derivative:

$$\frac{dD_{\text{EM}}}{dt} = \frac{dw_{\text{EM}}}{dt} \cdot u_{\text{t,net}} + w_{\text{EM}} \cdot \frac{du_{\text{t,net}}}{dt}. \tag{128}$$

Since $w_{\text{EM}}$ is established by the fields, the dominant term is:

$$\frac{dD_{\text{EM}}}{dt} = w_{\text{EM}}(t) \cdot a_{\text{t,net}}(t), \tag{129}$$

$$dD_{\text{EM}} = w_{\text{EM}}(t) \cdot du_{\text{t,net}}. \tag{130}$$

*Thrust.* The energy density is defined as the energy confined within a volume, associated with the boundary surface of that volume,

$$A_{\partial V} = \oint_{\partial V} dA.$$

Multiplying the inner boundary surface of the waveguide,

$$A_{\partial V} \approx 2\pi r \cdot 2\pi r_c,$$

with the preceding expression (Eq. (130)) yields the confined power that propagates azimuthally along the toroidal axis

$$A_{\partial V} \cdot dD_{\text{EM}} = A_{\partial V} \cdot w_{\text{EM}}(t) \cdot du_{\text{t,net}}. \tag{131}$$

Dividing by $u_g$ yields the thrust:

$$F_{\text{thrust}}(t) = A_{\partial V} \cdot w_{\text{EM}}(t) \cdot \frac{du_{\text{t,net}}}{u_g} = A_{\partial V} \cdot w_{\text{EM}}(t) \cdot \frac{a_{\text{t,net}}(t)}{a_g},$$

$$a_{\text{t,net}}(t) = \frac{du_{\text{t,net}}}{dt} = -\frac{2}{k} \cdot \frac{d^2\phi}{dt^2} = -2u_g \cdot \frac{d\omega}{2\pi}, \tag{132}$$

where $a_g = u_g/T$ is the maximum group-velocity-limited acceleration. **Important:** $a_{\text{t,net}}(t)$ denotes the net tangential acceleration of the standing wave, *not* the resulting thrust. Thus,

$$F_{\text{EM}}(t) = F_{\text{thrust}}(t) = -2A_{\partial V} \cdot w_{\text{EM}}(t) \cdot \frac{d\omega}{\omega_g}. \tag{133}$$

When the velocity change equals $u_g$, corresponding to an angular velocity shift of $\omega_g$, the thrust reaches its peak. Expressing this as a discrete angular velocity shift $\Delta\omega$ over interval $T$, we obtain:

$$F_{\text{EM}} = F_{\text{thrust}} = -2A_{\partial V} \cdot w_{\text{EM}} \cdot \frac{\Delta\omega}{\omega_g}. \tag{134}$$

Using representative parameters: waveguide boundary surface $A_{\partial V} \approx 0.335\,\text{m}^2$, energy density $w_{\text{EM}} = 10\,\text{J/m}^3$, and angular velocity shift $\pm\omega_g/2$, we obtain:

$$F_{\text{EM}} \approx \mp 2 \cdot 0.335 \cdot 10 \cdot \frac{1}{2} \approx \mp 6.708\,\text{N}. \tag{135}$$

For system mass $M = 1$ kg, the system acceleration becomes:

$$a = \frac{F_{\text{EM}}}{M} \approx \mp 6.708\,\text{m/s}^2. \tag{136}$$

Increasing $w_{\text{EM}}$ to $1000\,\text{J/m}^3$ yields:

$$F_{\text{thrust}} \approx \mp 670.8\,\text{N}. \tag{137}$$

*Electric Field Strength.* Assuming energy stored solely in the electric field:

$$w_{\mathrm{EM}} \approx \varepsilon_0 E^2 \quad \Rightarrow \quad E \approx \sqrt{\frac{w_{\mathrm{EM}}}{\varepsilon_0}}, \tag{138}$$

$$w_{\mathrm{EM}} = 10 \quad \Rightarrow \quad E \approx 1.0627 \cdot 10^6 \,\mathrm{V/m}, \tag{139}$$

$$w_{\mathrm{EM}} = 1000 \quad \Rightarrow \quad E \approx 1.0627 \cdot 10^7 \,\mathrm{V/m}. \tag{140}$$

Corresponding displacement field:

$$D = \varepsilon_0 E, \tag{141}$$

$$D = 9.410 \cdot 10^{-6} \,\mathrm{C/m^2}, \tag{142}$$

$$D = 9.410 \cdot 10^{-5} \,\mathrm{C/m^2}. \tag{143}$$

In toroidal TE-mode, $E$ arises from stored energy, not charge drift. The displacement field $D$ serves as a proxy for the effective charge distribution sustaining the field. Hypothetical translation of $D$ around the ring—following the same velocity and phase acceleration—would induce equivalent thrust via momentum transfer. This highlights that thrust arises from dynamic energy and momentum density, not from charge motion.

*Electromagnetic Polaritons.* Polaritons traditionally couple EM fields to lattice vibrations or excitons. Here, each standing wave acts as a self-confined polariton—an excitation coupled to its own trapped energy density, independent of material dipoles. This purely field-based structure exhibits effective mass and inertial response, enabling directional thrust via phase modulation.

To our knowledge, this formulation of a self-confined electromagnetic polariton—defined by field–energy coupling within a resonant geometry and exhibiting inertial behavior—has not been formally introduced. It extends the polariton paradigm into a purely electromagnetic regime, enabling thrust without material coupling and establishing a new class of macroscopic polaritons.

From Eq. (134), a massless inertia-equivalent entity emerges (the $E\sqrt{\varepsilon_0 \varepsilon_{g_0}}$ is discussed in a subsequent section). Replacing confined energy density with an inertial proxy, each standing wave behaves as a virtual mass carrier. The effective EM mass can be exposed by setting $\Delta\omega = \omega_g$:

$$m_{\mathrm{EM}} = \frac{F_{\mathrm{EM}}}{2a_{\mathrm{EM}}} = \frac{2A_{\partial V} \cdot w_{\mathrm{EM}}}{2E\sqrt{\varepsilon_0 \varepsilon_{g_0}}} = A_{\partial V} \cdot E\sqrt{\frac{\varepsilon_0}{\varepsilon_{g_0}}}, \tag{144}$$

where $\varepsilon_{g_0} = 4\pi G$ is the gravitational permittivity. For representative energy densities:

$$w_{\mathrm{EM}} = 10 \Rightarrow m_{\mathrm{EM}} \approx 3.66 \cdot 10^4 \,\mathrm{kg},$$
$$w_{\mathrm{EM}} = 10 \Rightarrow a_{\mathrm{EM}} \approx \mp 9.158 \cdot 10^{-5} \,\mathrm{m/s^2},$$
$$w_{\mathrm{EM}} = 1000 \Rightarrow m_{\mathrm{EM}} \approx 3.66 \cdot 10^5 \,\mathrm{kg},$$
$$w_{\mathrm{EM}} = 1000 \Rightarrow a_{\mathrm{EM}} \approx \mp 9.158 \cdot 10^{-4} \,\mathrm{m/s^2}.$$

This inertial framing allows EM standing waves to act as mechanically active agents in closed-field propulsion models.

## VII. ELECTROMAGNETIC INERTIAL DRIVE (TOROIDAL COILS)

An experimentally accessible configuration involves two toroidal coils, each wound around a dedicated iron or ferrite core (see FIG. 9). Unlike GHz-range resonators, this setup operates in the ultra-low to very-low frequency (ULF–VLF) range, approximately 0.001 Hz to 30 kHz, where acoustic power amplifiers are readily available. The ring topology supports counter-propagating standing waves, and a time-dependent phase shift modulates these waves to produce net tangential acceleration and thrust.

In TE-mode resonators using high-permeability materials such as MnZn ferrites, magnetic energy dominates. For each identical toroidal coil, the electromagnetic energy density simplifies to:

$$w_{\mathrm{EM}} = \left(\frac{1}{2}\varepsilon E^2 + \frac{1}{2}\mu H^2\right) \approx \mu H^2 \approx \frac{B^2}{\mu_0 \mu_r}, \tag{145}$$

where $B = \mu_0 \mu_r H$. This holds when $\mu_r \gg 1$, allowing the electric term to be replaced with an equal amount of magnetic energy density.

The same applies to laminated iron cores under low-frequency excitation, where TE-mode confinement ensures the magnetic field remains azimuthal. Despite iron's conductivity and eddy current susceptibility at higher frequencies, its magnetic response in the ULF–VLF range remains strong enough to justify magnetic-dominant modeling.

In TE modes:

$$\text{TE mode}: \quad E_z = 0, \quad H_\phi \neq 0, \tag{146}$$

maximizing magnetic energy storage and matching ferrite properties. TM modes, which rely on axial electric fields, are less effective in magnetically active media.

*Magneto-Polaritons.* When a ferrite ring supports a magneto-polariton—a hybrid excitation of EM fields and magnetic dipoles—the system acquires an effective rest mass from stored field energy. This mass is not mechanical, but energy-equivalent.

To quantify dipole participation, we introduce a coupling factor $\kappa_m$ for each standing wave:

$$m_{\mathrm{EM}} = \frac{F_{\mathrm{EM}}}{2a_{\mathrm{EM}}} = m_{\mathrm{rest}} = \kappa_m \cdot \frac{2A_{\partial V} \cdot w_{\mathrm{EM}}}{2B/u_g \mu_r \sqrt{\mu_0 \mu_{i_0}}} \tag{147}$$

$$= \kappa_m \cdot A_{\partial V} \cdot B \cdot u_g \sqrt{\frac{\mu_{i_0}}{\mu_0}}, \tag{148}$$

where $A_{\partial V}$ is the boundary surface of the ring (torus), $u_g$ group velocity, (the $B/u_g \mu_r \sqrt{\mu_0 \mu_{i_0}}$ is discussed in a subsequent section), and $\kappa_m \in [0, 1]$ reflects field–dipole coupling strength.

Let us assume a ferrite or laminated iron ring of radius $r$, biased by a static field $\vec{H}_0 = H_0 \hat{z}$, inducing magnetization $\vec{M} = \chi_m \vec{H}$. The EM field couples to these dipoles, forming a bulk magneto-polariton that stores energy and exhibit inertial response. For MnZn ferrites, $\chi_m \sim 10^3$–$10^4$, yielding similar $\mu_r$. The magnetic response follows:

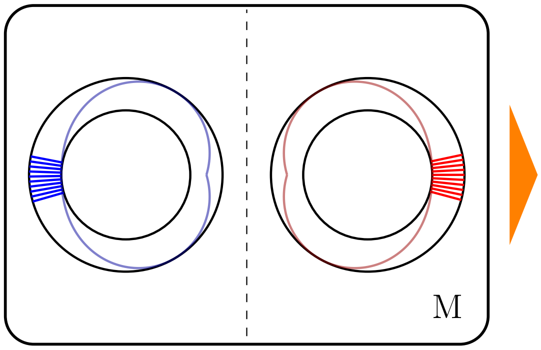


FIG. 9. **Electromagnetic Inertial Drive.** Analog to the mechanical inertial drive, using toroidal coils with iron or ferrite cores. Counter-propagating standing waves are confined within the ring—blue for CW, red for CCW. A time-dependent phase shift modulates these waves, producing net tangential acceleration (orange arrow) along the $x$-axis, inducing linear thrust on system $M$.

$$\vec{B} = \mu_0(\vec{H} + \vec{M}), \quad \vec{M} = \chi_m \vec{H}. \tag{149}$$

The dominant field component is the azimuthal magnetic field $H_\phi(\phi, t)$, circulating around the ring. Here, $\phi$ is the geometric azimuthal angle, and $\phi(t)$ the time-dependent phase shift.

Embedding a standing wave into circular geometry requires its spatial structure to track angular displacement. We define:

$$H_\phi(\phi(t), t) = H_0 \sin(kr\phi(t)) \cos(\omega t), \tag{150}$$

where $k = \frac{n}{r}$ is the azimuthal wavenumber and $r$ the ring radius.

Define a radial displacement field $y_\phi(\phi(t), t)$ as:

$$y_\phi(\phi(t), t) = \mathcal{F}[H_\phi(\phi(t), t)], \tag{151}$$

where $\mathcal{F}[\cdot]$ maps field amplitude to physical displacement.

The excitation's position vectors (CW: $-\cos(\phi(t))$, CCW: $+\cos(\phi(t))$) are:

$$\vec{R}_{\mathrm{rr}}(t) = \left[r + y_\phi(\phi(t), t)\right] \begin{pmatrix} \mp\cos(\phi(t)) \\ \sin(\phi(t)) \\ 0 \end{pmatrix}, \tag{152}$$

embedding wave-modulated displacement into ring curvature. For resonance:

$$r + y_\phi(\phi(t), t) = \frac{1}{k}, \tag{153}$$

linking wave geometry to the system's inertial scale.

The net tangential acceleration is

$$\vec{a}_{\mathrm{t,net}}(t) = -\frac{2}{k} \cdot \frac{d^2\phi}{dt^2} \begin{pmatrix} \sin(\phi(t)) \\ 0 \\ 0 \end{pmatrix}, \tag{154}$$

arising from curvature-coupled dynamics of the magneto-polariton envelope. This acceleration acts as a self-contained carrier, with the confined energy density providing the thrust force and resulting acceleration.

TABLE I. **MnZn Ferrite Core Toroid T87/56/13 3E6 Grade**

| **Parameter** | **Value** |
|---|---|
| Special Conductivity ($\sigma$) | $10\,\mathrm{S/m}$ |
| Initial Rel. Magnetic Permeability ($\mu_r$) | 10000 |
| Density ($\rho$) | $4900\,\mathrm{kg/m^3}$ |
| mass ( $M$) | $0.2\,\mathrm{kg}$ |
| Effective Cross-sectional area ($A$) | $1.94 \cdot 10^{-4}\,\mathrm{m^2}$ |
| Effective volume ($V$) | $42.133 \cdot 10^{-6}\,\mathrm{m^3}$ |
| Effective Cross-sectional radius ($r_c$) | $0.00786\,\mathrm{m}$ |
| Effective Toroidal radius ($r$) | $0.0345\,\mathrm{m}$ |
| Effective length ($L$) | $0.2172\,\mathrm{m}$ |

Consider a system composed of two identical toroidal coils, each wound around a ferrite core (see TABLE I) with an approximately circular cross section of radius $r_c$, as illustrated in FIG. 9.

In highly conductive, magnetically permeable media—such as laminated iron under low-frequency excitation—the electromagnetic phase velocity is significantly reduced due to material properties and excitation geometry. In the monochromatic regime, where frequency is fixed and narrowband, group velocity $u_\mathrm{g}$ and phase velocity $u_\mathrm{p}$ converge. The effective propagation speed of an EM wave is:

$$u_\mathrm{g} \approx u_\mathrm{p} = \left[\frac{\varepsilon\mu}{2}\left(\sqrt{1 + \left(\frac{\sigma}{\omega\varepsilon}\right)^2} - 1\right)\right]^{-1/2}, \tag{155}$$

$$\sigma \gg \omega\varepsilon \quad \Rightarrow \quad \sqrt{1 + \left(\frac{\sigma}{\omega\varepsilon}\right)^2} - 1 \approx \frac{\sigma}{\omega\varepsilon}, \tag{156}$$

$$u_\mathrm{g} \approx \left(\frac{\mu\sigma}{4\pi f}\right)^{-1/2}. \tag{157}$$

This approximation holds in weakly dispersive media and remains valid for thrust modeling in ferrite or iron-core systems.

Guided wavelength required for resonance:

$$\lambda_\mathrm{g} \approx L. \tag{158}$$

Toroids are excited by a magnetic field strength $H \approx 65\,\mathrm{A/m}$. From the datasheet B–H curve:

$$B \approx 0.35\,\mathrm{T} \quad \Rightarrow \quad \mu_{\mathrm{r,eff}} \approx \frac{B}{\mu_0 H} \approx 4284. \tag{159}$$

At excitation frequency $f = 4.96\,\mathrm{kHz}$:

$$u_\mathrm{g} \approx \left(\frac{4\pi f}{\mu_{\mathrm{r,eff}}\sigma}\right)^{1/2} \approx 1075\,\mathrm{m/s}, \tag{160}$$

$$\lambda_\mathrm{g} \approx \frac{u_\mathrm{g}}{f} \approx 0.2169\,\mathrm{m}. \tag{161}$$

The associated magnetic energy density is:

$$w_{\mathrm{EM}} \approx \frac{B^2}{\mu_0 \mu_{\mathrm{r,eff}}} \approx 22.75\,\mathrm{J/m^3}. \tag{162}$$

For angular velocity shift $\Delta\omega = \pm\omega_g/2$ and $A_{\partial V} \approx 2\pi r_c \cdot L \approx 0.0107\,\mathrm{m}^2$, thrust becomes:

$$F_{\mathrm{EM}} = F_{\mathrm{thrust}} = -2A_{\partial V} \cdot \frac{B^2}{\mu_0\mu_{\mathrm{r,eff}}} \cdot \frac{\Delta\omega}{\omega_g} \approx \mp 0.488\,\mathrm{N},$$
$$a = \frac{F_{\mathrm{thrust}}}{M} \approx \mp 0.488\,\mathrm{m/s}^2.$$

And the effective electromagnetic mass per bulk magneto-polariton toroid, under the assumption of field–dipole coupling, $\kappa_{\mathrm{m}} \approx 1.0$:

$$m_{\mathrm{EM}} = \kappa_m \cdot A_{\partial V} \cdot B \cdot u_g \sqrt{\frac{\mu_{i_0}}{\mu_0}} \approx 0.415\,\mathrm{kg}, \quad (163)$$

$$a_{\mathrm{EM}} = \frac{B}{u_g \mu_r \sqrt{\mu_0 \mu_{i_0}}} \approx \mp 0.588\,\mathrm{m/s}^2. \quad (164)$$

## VIII. VALIDATION PROTOCOL FOR INERTIAL DRIVE SYSTEMS

TABLE II. Validation Criteria for Inertial Drive Systems

| **Criterion** | **Requirement** |
|---|---|
| Isolated Test System | Operation must be orthogonal to gravity to eliminate gravitational coupling. |
| Curved Component Motion | Components must follow curved trajectories—circular, elliptical, or helical. |
| Paired Component Symmetry | A pair of components must undergo mirrored acceleration profiles along symmetric paths (e.g., in the $x$–$y$ plane). |
| Non-Uniform Velocity Profile | Motion must exhibit time-dependent acceleration or deceleration. |
| Component Type | Includes both massive bodies and massless entities (e.g., standing waves, fields, or trapped energy density). |
| Internal Energy Source | All power and thrust must originate within the system's own frame of reference. |
| Surface Corridor Test | Requires a lubricated track at least $10\times$ the device length in the thrust direction. |
| Velocity Benchmark | Final velocity must exceed twice the initial-cycle velocity. |
| Orthogonal Thrust Vector | Thrust must act perpendicular to the excitation axis (e.g., excitation along $y$, thrust along $x$). |
| Thrust Efficiency | Tangential force must exceed radial or centripetal components by a factor of at least 1. |

## IX. PODKLETNOV GRAVITY SHIELDING EXPERIMENT

Podkletnov's experimental setup featured a high-temperature superconducting disc, typically $YBa_2Cu_3O_{7-x}$, cooled below its critical temperature and excited by short magnetic pulses applied perpendicular to its surface.

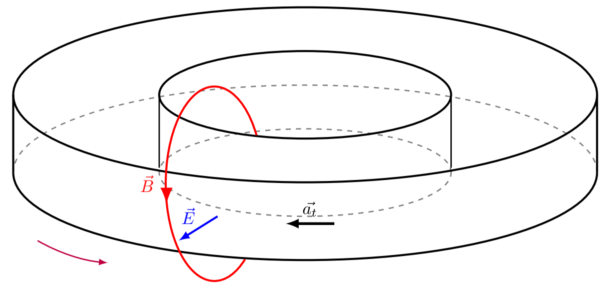


FIG. 10. **Rotating Superconductor.** A superconducting toroidal disc excited by a short magnetic pulse. Upon entering the superconducting state, induced supercurrents circulate circumferentially, expelling the applied field and establishing a static poloidal topology $\vec{B}$ (red). When the rotating disc at constant speed undergoes a smooth tangential deceleration $\vec{a}_t$, it generates an azimuthal thrust—gravitational or inertia-like—arising from the deceleration of the translated $\vec{B}$-field energy density.

The disc was often rotated, and the configuration reportedly produced anomalous effects above the superconductor, including weak gravitational shielding.

While these claims remain controversial, the geometry and excitation method suggest a nontrivial interaction between induced currents and expelled magnetic fields.

This work proposes that the disc behaves not as a flat superconductor, but as a toroidal-like structure in current geometry. Perpendicular excitation induces azimuthal supercurrents—circulating circumferentially within the surface. Upon entering the superconducting state, these currents expel the applied field and establish a poloidal magnetic topology: field lines emerge from the inner radius, curve outward across the surface, and return beneath the disc. The resulting flux shell is perpendicular to the azimuthal direction, with the superconductor acting as a flux-excluding core embedded in a curved poloidal field (see FIG. 10).

Consider a superconducting disc rotating with angular velocity $\vec{\omega}(t)$, carrying a static poloidal magnetic field $\vec{B}(\vec{r})$ that co-rotates with the disc. The field remains stationary in the rotating frame, and the local tangential velocity at radius $r$ is:

$$\vec{u}_t(t) = \vec{\omega}(t) \times \vec{r}. \quad (165)$$

Even without free charges, motion through the lab frame induces a motional electric field:

$$\vec{u}_t(t) \perp \vec{B}(\vec{r}) \Rightarrow \vec{E} = -\vec{u}_t(t) \times \vec{B}(\vec{r}). \quad (166)$$

This is justified by the fact that the expelled magnetic field, when set into rotation, induces an external motional electric field through the homopolar Faraday mechanism.

To track how $\vec{E}$ evolves, we apply the total derivative along the source trajectory:

$$\frac{d\vec{E}}{dt} = -\left(\frac{d\vec{u}_t}{dt} \times \vec{B} + \vec{u}_t \times \frac{d\vec{B}}{dt}\right). \tag{167}$$

Expanding the magnetic field derivative:

$$\frac{d\vec{B}}{dt} = \frac{\partial \vec{B}}{\partial t} + (\vec{u}_t \cdot \nabla)\vec{B}, \tag{168}$$

we obtain the full evolution:

$$\frac{d\vec{E}}{dt} = -\left(\frac{d\vec{u}_t}{dt} \times \vec{B} + \vec{u}_t \times \left(\frac{\partial \vec{B}}{\partial t} + (\vec{u}_t \cdot \nabla)\vec{B}\right)\right). \tag{169}$$

This total derivative contains three contributions:

$$\begin{aligned} \frac{d\vec{E}}{dt} = &-\overbrace{\frac{d\vec{u}_t}{dt} \times \vec{B}}^{\text{source acceleration}} \\ &-\overbrace{\vec{u}_t \times \frac{\partial \vec{B}}{\partial t}}^{\text{time-varying field}} \\ &-\overbrace{\vec{u}_t \times (\vec{u}_t \cdot \nabla)\vec{B}}^{\text{spatial nonuniformity}}. \end{aligned} \tag{170}$$

Each term corresponds to a distinct mechanism: acceleration of the source, motion through a time-varying field, and spatial nonuniformity in $\vec{B}$. This decomposition isolates the drivers of motional field evolution and thrust generation across rotating superconductors, translating coils, and time-modulated field setups.

Building on the kinematic definition of $\vec{E}$, we also express its total derivative as:

$$\frac{d\vec{E}}{dt} = \frac{\partial \vec{E}}{\partial t} + (\vec{u}_t \cdot \nabla)\vec{E}. \tag{171}$$

The total derivative of the motional electric field $\vec{E}$ describes its evolution along the trajectory of a moving source. It accounts for both explicit time dependence and spatial variation due to motion. Here, $\vec{u}_t(t)$ is the tangential velocity of the rotating source, and the second term captures how the field changes as the source moves through space.

In our configuration, both $\vec{E}$ and $\vec{B}$ are time-independent. From Eqs. (169) and (171):

$$-\vec{u}_t \times \frac{\partial \vec{B}}{\partial t} = \vec{0}, \quad \frac{\partial \vec{E}}{\partial t} = \vec{0}. \tag{172}$$

Moreover, the term $\vec{u}_t \times \left((\vec{u}_t \cdot \nabla)\vec{B}\right)$ vanishes. The expelled magnetic field $\vec{B}$ is poloidal, static, and spatially confined, with no azimuthal dependence. Since $\vec{u}_t$ is purely tangential:

$$(\vec{u}_t \cdot \nabla)\vec{B} = \vec{0}. \tag{173}$$

Equating Eqs. (169) and (171), the surviving term yields:

$$(\vec{u}_t \cdot \nabla)\vec{E} = -\frac{d\vec{u}_t}{dt} \times \vec{B}. \tag{174}$$

Integrating over time:

$$\vec{E}_m(t) = \int_0^t (\vec{u}_t(t') \cdot \nabla)\vec{E}\, dt' = -\int_0^t \left(\frac{d\vec{u}_t}{dt'} \times \vec{B}\right) dt'. \tag{175}$$

Assuming $\vec{B}$ is static and $\vec{u}_t(0) = \vec{0}$:

$$\vec{E}_m(t) = -\vec{u}_t(t) \times \vec{B}, \tag{176}$$

representing the accumulated motional electric field from tangential acceleration through the trapped magnetic shell.

The expelled poloidal field forms a static electromagnetic shell around the disc, resembling a standing wave structure. The superconductor acts as a flux-excluding core. Rotation induces:

$$\vec{E}_m(t) = -\vec{u}(t) \times \vec{B},$$

where $\vec{u}(t)$ is tangential velocity and $\vec{B}$ the expelled field. Though $\vec{B}$ is static, rotation sweeps through spatial gradients, building electric energy density.

Total electromagnetic energy density:

$$w_{\text{EM}}(t) = \frac{1}{2}\varepsilon_0 |\vec{E}_m(t)|^2 + \frac{1}{2\mu_0}|\vec{B}|^2. \tag{177}$$

Assuming confinement to the poloidal volume:

$$U_{\text{EM}}(t) = \int_{V_{\text{poloidal}}} \left(\frac{1}{2}\varepsilon_0 |\vec{E}_m(t)|^2 + \frac{1}{2\mu_0}|\vec{B}|^2\right) dV. \tag{178}$$

In field propulsion, the change in trapped energy yields thrust-like force:

$$F_{\text{thrust}} = \frac{1}{u_g} \cdot \frac{dU_{\text{EM}}}{dt}, \tag{179}$$

where $u_g$ is the effective translational velocity of the energy density.

To estimate $u_g$, we use Podkletnov's 1997 setup: a toroidal disc with diameter $D = 275$ mm, giving:

$$\lambda_g \approx L = 2\pi \cdot \frac{D}{2} \approx 0.863\,\text{m}. \tag{180}$$

The energy is confined to the external shell, not within the disc. For 5000 rpm:

$$f = \frac{5000}{60} \approx 83.3\,\text{Hz}, \quad u_g = \lambda_g f \approx 71.8\,\text{m/s}. \tag{181}$$

Theoretical upper bound for disc tangential acceleration:

$$a_g = \frac{u_g}{T} = u_g \cdot f \approx 5981\,\text{m/s}^2. \tag{182}$$

Analogous to microwave setups, thrust from the trapped shell:

$$F_{\text{thrust}}(t) = A_{\partial V} \cdot w_{\text{EM}}(t) \cdot \frac{a_{\text{t}}(t)}{a_g} = A_{\partial V} \cdot w_{\text{EM}}(t) \cdot \frac{\omega(t)}{\omega_g}. \quad (183)$$

where, $A_{\partial V}$ denotes the boundary surface area associated with the volume of the poloidal field, $w_{\text{EM}}(t)$ the instantaneous energy density, $a_{\text{t}}(t)$ the tangential acceleration, and $a_g$ the maximum acceleration.

Consider a scenario where thrust acts vertically, counteracting gravity. Assume the disc's rotational speed decreases from 5000 rpm to 3500 rpm. With poloidal cross-sectional radius $r_c = 0.05\,\text{m}$:

$$\omega_g = \frac{2\pi}{60} \cdot 5000 \approx 523.6\,\text{rad/s}, \quad (184)$$

$$\Delta\omega = \frac{2\pi}{60} \cdot (3500 - 5000) \approx -157\,\text{rad/s}, \quad (185)$$

$$A_{\partial V} \approx 2\pi r_c \cdot 2\pi(D/2) \approx 0.271\,\text{m}^2. \quad (186)$$

Assuming maximum motional field intensity:

$$|\vec{E}_m| \approx |\vec{u}_g \times \vec{B}| \approx 71.8\,\text{V/m}, \quad (187)$$

the electric energy density:

$$w_E \approx \varepsilon_0 |\vec{E}_m|^2 \approx 4.56 \cdot 10^{-8}\,\text{J/m}^3. \quad (188)$$

Magnetic energy density for $B = 0.1\,\text{T}$:

$$w_M \approx \frac{1}{\mu_0}|\vec{B}|^2 \approx 7.958 \cdot 10^3\,\text{J/m}^3. \quad (189)$$

Thus, motional electric energy is negligible, and:

$$w_{\text{EM}} \approx w_M \approx \frac{1}{\mu_0}|\vec{B}|^2. \quad (190)$$

Combining with Eq. (183), thrust becomes:

$$F_{\text{EM}} = F_{\text{thrust}} = -A_{\partial V} \cdot \frac{B^2}{\mu_0} \cdot \frac{a_t}{a_g} = -A_{\partial V} \cdot \frac{B^2}{\mu_0} \cdot \frac{\Delta\omega}{\omega_g}. \quad (191)$$

For $M = 1\,\text{kg}$, a 2.4% weight reduction implies:

$$a \approx 0.236\,\text{m/s}^2 \quad \Rightarrow \quad F_{\text{thrust}} \approx 0.236\,\text{N}, \quad (192)$$

yielding:

$$a_{\text{net}} = g - |a| \approx 9.574\,\text{m/s}^2, \quad (193)$$

$$a_{\text{net},\%} = \frac{g - |a|}{g} \cdot 100\% \approx 2.4\%. \quad (194)$$

Substituting into Eq. (191):

$$B \approx 1.91 \cdot 10^{-3}\,\text{T}, \quad w_{\text{EM}} \approx 2.903\,\text{J/m}^3. \quad (195)$$

Assuming $\Delta\omega$ occurs within $T = 1/f \approx 0.012\,\text{s}$:

$$a_t = a_g \cdot \frac{\Delta\omega}{\omega_g} \approx -1.79 \cdot 10^3\,\text{m/s}^2, \quad (196)$$

which is mechanically unfeasible.

Thus, angular velocity-based thrust is best suited for electromagnetic standing wave systems. Tangential acceleration remains applicable to both mechanical and EM mechanisms.

To match $w_{\text{EM}} \approx 2.903\,\text{J/m}^3$ in a rotating superconductor:

$$w_{\text{EM}} \approx \frac{B^2}{\mu_0} \cdot \frac{a_t}{a_g} \approx 2.903\,\text{J/m}^3. \quad (197)$$

Applying $B = 0.2\,\text{T}$:

$$B^2/\mu_0 \approx 3.183 \cdot 10^4\,\text{J/m}^3, \quad a_t \approx -0.545\,\text{m/s}^2. \quad (198)$$

The required deceleration time is:

$$\Delta t = \Delta\omega \cdot D/2a_t \approx 39.5\,\text{s}. \quad (199)$$

The associated electromagnetic mass and acceleration for $\kappa_{\text{m}} \approx 1.0$ and $\mu_r = 1$ is given by:

$$m_{\text{EM}} = \kappa_m \cdot A_{\partial V} \cdot B \cdot u_g \sqrt{\frac{\mu_{i_0}}{\mu_0}} \approx 3.833 \cdot 10^{-3}\,\text{kg}, \quad (200)$$

$$a_{\text{EM}} = \frac{B}{u_g \mu_r \sqrt{\mu_0 \mu_{i_0}}} \approx 2.055 \cdot 10^2\,\text{m/s}^2. \quad (201)$$

## X. ELECTROMAGNETIC COUPLING TO GRAVITATIONAL AND INERTIAL FIELDS

Central to the thrust expression is the electromagnetic energy density, which may be electric or magnetic:

$$F_{\text{EM}} = F_{\text{thrust}} = -2A_{\partial V} \cdot w_{\text{EM}} \cdot \frac{\Delta\omega}{\omega_g}. \quad (202)$$

Since this expression transfers momentum from motional field energy to mechanical momentum, it raises the question: could a corresponding energy density exist within a gravito-inertial framework?

*Electric Analogy.* Assuming purely electric energy density:

$$F_{\text{EM}} = F_{\text{thrust}} = -2A_{\partial V} \cdot w_{\text{E}} \cdot \frac{\Delta\omega}{\omega_g}, \quad (203)$$

$$-2A_{\partial V} \cdot w_{\text{E}_{\text{G}}} \cdot \frac{\Delta\omega}{\omega_g} = -2A_{\partial V} \cdot w_{\text{E}} \cdot \frac{\Delta\omega}{\omega_g}, \quad (204)$$

$$\frac{1}{2}\varepsilon_{g_0}\varepsilon_r E_G^2 = \frac{1}{2}\varepsilon_0 \varepsilon_r E^2 \Rightarrow E_G = \pm E\sqrt{\frac{\varepsilon_0}{\varepsilon_{g_0}}}, \quad (205)$$

$$a_{\text{EM}} = D_G = \varepsilon_{g_0}\varepsilon_r E_G = \pm E \varepsilon_r \sqrt{\varepsilon_0 \varepsilon_{g_0}}. \quad (206)$$

*Magnetic Analogy.* For magnetic energy density:

$$F_{\text{EM}} = F_{\text{thrust}} = -2A_{\partial V} \cdot w_{\text{M}} \cdot \frac{\Delta\omega}{\omega_g}, \quad (207)$$

$$\frac{B_I^2}{2\mu_{i_0}\mu_r} = \frac{B^2}{2\mu_0 \mu_r} \Rightarrow B_I = \pm B\sqrt{\frac{\mu_{i_0}}{\mu_0}}, \quad (208)$$

$$a_{\text{EM}} = D_I = \frac{1}{\mu_{i_0}\mu_r u_g} B_I = \pm \frac{B}{u_g \mu_r \sqrt{\mu_0 \mu_{i_0}}}. \quad (209)$$

These analogies were derived in [22], which extends Maxwell's equations to arbitrary charge types through a Gauss-like law for force flux:

$$\oint_{\partial V} \vec{F}_T \cdot d\vec{A} = \frac{q_T^2}{\varepsilon_{T_0}}. \tag{210}$$

Gravitational permittivity and inertial permeability:

$$\varepsilon_{g_0} = 4\pi G = 8.38717 \cdot 10^{-10}\,\mathrm{J/(kg^2 \cdot m)}, \tag{211}$$

$$\mu_{i_0} = 1/c^2\varepsilon_{g_0} = 1.32661 \cdot 10^{-8}\,(\mathrm{kg \cdot m^{-1} \cdot s})^2/(\mathrm{J \cdot m}). \tag{212}$$

Fields $D_G$ and $D_I$ carry units of N/kg and m/s$^2$, analogous to $D_E$.

*Field Equivalence.* Assuming $D_G = D_I = \pm 9.81\,\mathrm{m/s^2}$, $u_g = c$, $\varepsilon_r = 1$, and $\mu_r = 1$, we obtain:

$$E = \frac{D_G}{\sqrt{\varepsilon_0 \varepsilon_{g_0}}} \approx \pm 1.13838 \cdot 10^{11}\,\mathrm{V/m}, \tag{213}$$

$$B = c D_I \sqrt{\mu_0 \mu_{i_0}} \approx \pm 379.72\,\mathrm{T}. \tag{214}$$

Resulting energy densities:

$$w_\mathrm{E} = w_\mathrm{M} = \varepsilon_0 E^2/2 = B^2/2\mu_0 \approx 5.721 \cdot 10^{10}\,\mathrm{J/m^3}, \tag{215}$$

$$w_\mathrm{E} \cdot c = w_\mathrm{M} \cdot c \approx 1.716 \cdot 10^{19}\,\mathrm{W/m^2}. \tag{216}$$

*Electromagnetic Mass.* From Eq. (144), the effective mass:

$$m_\mathrm{EM} = \frac{F_\mathrm{EM}}{a_\mathrm{EM}} = \frac{A_{\partial V} \cdot w_\mathrm{EM}}{a_\mathrm{EM}} \cdot \frac{\Delta\omega}{\omega_g}. \tag{217}$$

Using $D_G$ and $D_I$ as thrust acceleration and $u_g = c$, $\varepsilon_r = 1$, and $\mu_r = 1$:

$$m_\mathrm{EM} = A_{\partial V} \cdot \frac{\Delta\omega}{2\omega_g} \left( \frac{\varepsilon_0 E^2}{D_G} + \frac{B^2}{\mu_0 D_I} \right), \tag{218}$$

yielding:

$$m_\mathrm{EM} = A_{\partial V} \cdot \frac{\Delta\omega}{2\omega_g} \left( E\sqrt{\frac{\varepsilon_0}{\varepsilon_{g_0}}} + cB\sqrt{\frac{\mu_{i_0}}{\mu_0}} \right). \tag{219}$$

This shows that a massless field structure can exhibit effective inertial effects under curved acceleration. When $w_\mathrm{E} = w_\mathrm{M}$, the magnetic or electric term may be replaced:

$$m_\mathrm{EM} = A_{\partial V} \cdot E\sqrt{\frac{\varepsilon_0}{\varepsilon_{g_0}}} \cdot \frac{\Delta\omega}{\omega_g} = A_{\partial V} \cdot cB\sqrt{\frac{\mu_{i_0}}{\mu_0}} \cdot \frac{\Delta\omega}{\omega_g}. \tag{220}$$

*Electron Analogy.* Let $A_{\partial V} = 4\pi r^2$ and $E$ the electron's or positron's electric field intensity at distance $r$:

$$m_\mathrm{EM} = \mp \frac{q_e}{\sqrt{\varepsilon_0 \varepsilon_{g_0}}} \cdot \frac{\Delta\omega}{\omega_g}, \tag{221}$$

$$m_g = \mp \frac{q_e}{\sqrt{\varepsilon_0 \varepsilon_{g_0}}} = \mp 1.85921 \cdot 10^{-9}\,\mathrm{kg}. \tag{222}$$

Dividing $m_g$ by Planck mass and squaring, we obtain the fine structure constant:

$$\alpha = \frac{q_e^2}{4\pi\varepsilon_0 \hbar c}, \tag{223}$$

$$\left(\frac{m_g}{m_p}\right)^2 = \alpha. \tag{224}$$

## XI. ALCUBIERRE WARP DRIVE

One of the most fascinating proposals in alternative propulsion is the Alcubierre warp drive (see FIG. 11). Formulated in 1994, it suggests that a spacecraft could achieve effective faster-than-light travel by contracting spacetime in front and expanding it behind—without violating local relativistic constraints. The ship remains stationary within a spacetime "bubble" that moves through the fabric of space.

Despite its elegance, the model faces major challenges: it requires exotic matter with negative energy density, immense energy, and raises questions about causality and stability. Nonetheless, it continues to inspire research into spacetime engineering.

*Warp Metric.* The line element defining the Alcubierre warp geometry is:

$$ds^2 = -c^2 dt^2 + [dx - v_s(t) f(r_s)\, dt]^2 + dy^2 + dz^2, \tag{225}$$

where $v_s(t)$ is the bubble velocity, $x_s(t)$ its center, and

$$r_s(t) = \sqrt{(x - x_s(t))^2 + y^2 + z^2}. \tag{226}$$

The shape function $f(r_s)$ defines the bubble profile:

$$f(r_s) = \frac{\tanh\left[\frac{r_s + R}{\delta}\right] - \tanh\left[\frac{r_s - R}{\delta}\right]}{2\tanh\left(\frac{R}{\delta}\right)}, \tag{227}$$

where $R$ is the bubble radius and $\delta$ the wall thickness.

*Coordinate Speed of Light.* For motion along $x$, the metric reduces to:

$$ds^2 = -c^2 dt^2 + [dx - v_s(t) f(r_s)\, dt]^2. \tag{228}$$

Setting $ds^2 = 0$ for light:

$$0 = -c^2 dt^2 + [dx - v_s(t) f(r_s)\, dt]^2, \tag{229}$$

$$\Rightarrow \frac{dx}{dt} = v_s(t) f(r_s) \pm c. \tag{230}$$

Inside the bubble ($f(r_s) \approx 1$), the coordinate speed becomes $v_s(t) \pm c$; outside ($f(r_s) \to 0$), it reduces to $\pm c$, recovering flat spacetime.

*Energy Requirements.* A simplified scaling estimate:

$$U_\mathrm{A} \approx \frac{c^2}{G} \cdot \frac{v^2 R^2}{\delta}, \tag{231}$$

where $v$ is the bubble velocity, $R$ its radius, and $\delta$ the wall thickness.

Assuming $v = 10c$, $R = 100\,\mathrm{m}$, $\delta = 1\,\mathrm{m}$:

$$U_\mathrm{A} \approx \frac{c^2}{G} \cdot \frac{(10c)^2 \cdot 100^2}{1} = \frac{c^4}{G} \cdot 10^6, \tag{232}$$

$$\frac{c^4}{G} \approx \frac{(3 \cdot 10^8)^4}{6.674 \cdot 10^{-11}} \approx 1.214 \cdot 10^{44}, \tag{233}$$

$$U_\mathrm{A} \approx 1.214 \cdot 10^{50}\,\mathrm{J}. \tag{234}$$

This corresponds to the mass-energy of several solar masses. Even under macroscopically reasonable assumptions, the energy demands are extreme.

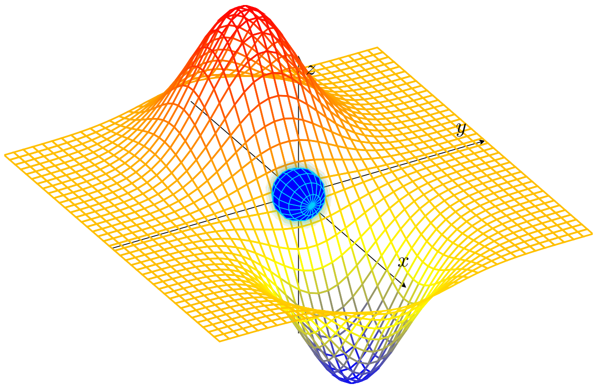


FIG. 11. **Alcubierre Warp Drive.** Spacetime contracts in front and expands behind the bubble. The ship remains stationary in the comoving frame, while the bubble moves through space.

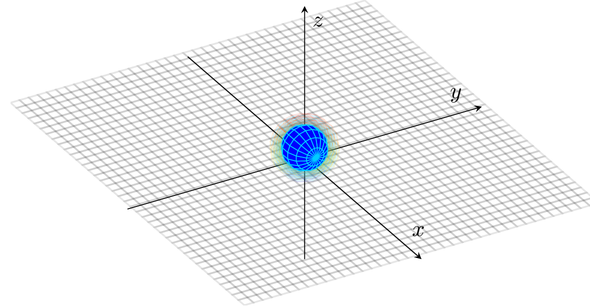


FIG. 12. **Inertial Warp Drive.** Accelerating, phase-locked standing waves propagate along the curved shell, inducing inertial shielding through proper time manipulation. Coordinate time remains unaffected inside the core. Rather than bending spacetime, the curved wave path modulates proper time to bend the inertial response.

From an engineering perspective, this energy must be precisely distributed to curve spacetime. The Einstein field equations require a tailored stress-energy tensor, localized in a thin shell with negative energy density to stabilize the bubble and enable superluminal motion. The feasibility of generating and sustaining such a configuration remains an open question.

## XII. INERTIAL WARP DRIVE

We propose an extension to special relativity—*inertial relativity*—that incorporates and generalizes its principles by introducing velocity-dependent modifications to the spacetime metric arising from internal propulsion mechanisms. Specifically, we examine how tangential acceleration of confined standing waves induces inertial shielding (see FIG. 12), suppressing proper time relative to coordinate time. This reduces inertial coupling to the external universe and leads to a localized reduction in the proper-time-defined speed of light along the shell where wave confinement occurs.

In the absence of shielding, the Minkowski line element is:

$$ds^2 = -c^2dt^2 + dx^2 + dy^2 + dz^2. \tag{235}$$

Assuming motion only along $x$:

$$ds^2 = -c^2dt^2 + dx^2. \tag{236}$$

Let $dx = u\,dt$:

$$ds^2 = (-c^2 + u^2)dt^2. \tag{237}$$

Relating to proper time:

$$-c^2d\tau^2 = (-c^2+u^2)dt^2 \quad \Rightarrow \quad \frac{d\tau}{dt} = \sqrt{1-\frac{u^2}{c^2}} = \frac{1}{\gamma}. \tag{238}$$

The inertial shielding concept involves a reduction of the local propagation rate. This effect arises from a pair of counter-propagating, accelerating standing waves that effectively isolate the system's inertia from the rest of the universe.

When a wave propagates along a curved waveguide of arc length $L$ (see FIG. 16), it reflects periodically, forming a closed-loop standing wave. Let $u_{\mathrm{sw}}(t)$ denote the instantaneous tangential velocity of the standing wave, driven by phase modulation $\phi(t)$.

Round-trip time:

$$t_{\mathrm{total}} = \frac{L}{c - u_{\mathrm{sw}}(t)} + \frac{L}{c + u_{\mathrm{sw}}(t)} = \frac{2Lc}{c^2 - u_{\mathrm{sw}}(t)^2}. \tag{239}$$

Effective round-trip speed:

$$u_{\mathrm{light}}(t) = \frac{2L}{t_{\mathrm{total}}} = c\left(1 - \frac{u_{\mathrm{sw}}(t)^2}{c^2}\right), \tag{240}$$

Applying the above expression to both clockwise (blue) and counterclockwise (red) waves in FIG. 16, and introducing a scaling energy factor on the ratio $n_s u_{\mathrm{sw}}/n_s c$, we define the net effective round-trip speed as

$$u_{\mathrm{light}}(t) = \frac{2L}{t_{\mathrm{total}}} = c\left(1 - \frac{u_{\mathrm{t,net}}(t)^2}{n_s^2 c^2}\right), \tag{241}$$

which reflects a locally reduced propagation rate due to inertial confinement. The shell's tangential velocity $u_{\mathrm{t,net}}$ and scaling factor $n_s$ define the inertial structure responsible for this deviation, corresponding to a shell-induced local metric distortion—without invoking spacetime curvature.

At $u_{\mathrm{t,net}}(t) = 0$:

$$t_{\mathrm{forward}} = t_{\mathrm{backwards}} = \frac{L}{c}, \quad t_{\mathrm{total}} = \frac{2L}{c}, \quad u_{\mathrm{light}} = c.$$

When $u_{\mathrm{sw}}(t) \neq 0$, timing becomes asymmetric. The expression remains valid as an instantaneous snapshot, capturing non-inertial modulation. Crucially, $c$ remains invariant; the shell behaves as a dynamic inertial medium, not a curved metric.

This velocity arises from phase-driven motion of the interference pattern and is governed by an energy factor $n_s \geq 1$, defined via:

$$m := m_{\mathrm{EM}} \Rightarrow U_s := V_{\mathrm{EM}} \cdot w_{\mathrm{EM}} = n_s^2 mc^2, \tag{242}$$

where $m$ here refers not to the bare rest mass of special relativity, but to an excited electromagnetic mass $m_{\mathrm{EM}}$ within volume $V_{\mathrm{EM}}$.

The net tangential velocity scales as:

$$u_{\mathrm{t,net}} = n_s c \cdot \frac{\Delta\omega}{\omega_g} = n_s c \cdot \frac{\Delta\phi}{\pi}. \tag{243}$$

To incorporate this locally reduced propagation rate (Eq. (241)) into the line element of the metric, we scale the metric by $n_s^2$ to reflect elevated energy density:

$$ds^2 = -n_s^2 c^2 d\tau^2 \left(1 - \frac{u_{\mathrm{t,net}}^2}{n_s^2 c^2}\right)^2, \tag{244}$$
$$ds^2 = -n_s^2 c^2 dt^2 + n_s^2 dx^2.$$

Substituting $n_s dx = u\, dt$:

$$ds^2 = -n_s^2 c^2 dt^2 + u^2 dt^2, \tag{245}$$

and relating to proper time:

$$-n_s^2 c^2 d\tau^2 \left(1 - \frac{u_{\mathrm{t,net}}^2}{n_s^2 c^2}\right)^2 = \left[-n_s^2 c^2 + u^2\right] dt^2. \tag{246}$$

Divide by $-n_s^2 c^2$:

$$d\tau^2 \left(1 - \frac{u_{\mathrm{t,net}}^2}{n_s^2 c^2}\right)^2 = \left[1 - \frac{u^2}{n_s^2 c^2}\right] dt^2, \tag{247}$$

yielding:

$$\frac{dt}{d\tau} = \left(1 - \frac{u_{\mathrm{t,net}}^2}{n_s^2 c^2}\right) \cdot \frac{1}{\sqrt{1 - \frac{u^2}{n_s^2 c^2}}}. \tag{248}$$

This shows that proper time is suppressed both by Lorentz motion and by shielding. When $n_s = 1$ and $u_{\mathrm{t,net}} = 0$, we recover standard time dilation. When $n_s > 1$, internal propulsion amplifies the effect, enabling relativistic motion without without reliance on external spacetime curvature e.g. gravitational fields.

*Relativistic Energy.* Total relativistic energy scales with the ratio of coordinate time to proper time:

$$U = m_i c^2 = mc^2 \cdot \frac{dt}{d\tau} = \gamma_s mc^2 \cdot \left(1 - \frac{u_{\mathrm{t,net}}^2}{n_s^2 c^2}\right), \tag{249}$$

where $\gamma_s = \left(1 - \frac{u^2}{n_s^2 c^2}\right)^{-1/2}$. Energy remains real and bounded; full shielding ($u_{\mathrm{t,net}} \to n_s c$) yields $m_i = 0$.

To examine light propagation, compare two forms of the interval:

$$ds^2 = -n_s^2 c^2 d\tau^2 \left(1 - \frac{u_{\mathrm{t,net}}^2}{n_s^2 c^2}\right)^2, \tag{250}$$
$$ds^2 = -n_s^2 c^2 dt^2 + n_s^2 dx^2.$$

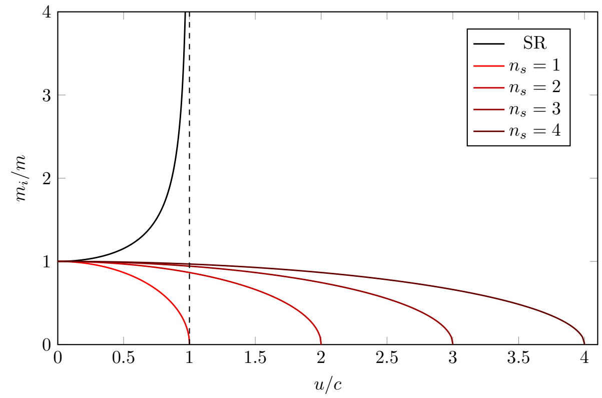


FIG. 13. **Relativistic Mass/Inertia.** In special relativity, inertial mass diverges as $u \to c$. In inertial shielding, mass vanishes as $u \to n_s c$, reframing mass as a bounded, field-coupled response.

Imposing $ds^2 = 0$:

$$-n_s^2 c^2 dt^2 + n_s^2 dx^2 = 0 \quad \Rightarrow \quad \left(\frac{dx}{dt}\right)_{\mathrm{light}} = c, \tag{251}$$

preserving Lorentz invariance externally.

*Transition to Proper Time.* For a stationary observer ($dx = 0$):

$$ds^2 = -n_s^2 c^2 dt^2, \tag{252}$$
$$ds^2 = -n_s^2 c^2 d\tau^2 \left(1 - \frac{u_{\mathrm{t,net}}^2}{n_s^2 c^2}\right)^2. \tag{253}$$

Equating:

$$dt = d\tau \left(1 - \frac{u_{\mathrm{t,net}}^2}{n_s^2 c^2}\right). \tag{254}$$

The proper-time-based displacement of light follows from applying the chain rule to the coordinate speed and the time conversion:

$$\left(\frac{dx}{d\tau}\right)_{\mathrm{light}} = \left(\frac{dx}{dt}\right)_{\mathrm{light}} \cdot \frac{dt}{d\tau} \tag{255}$$

*Proper-Time-Based Speed of Light.* Coordinate displacement per unit proper time:

$$\left(\frac{dx}{d\tau}\right)_{\mathrm{light}} = c \cdot \left(1 - \frac{u_{\mathrm{t,net}}^2}{n_s^2 c^2}\right). \tag{256}$$

Although the system undergoes acceleration, it remains inertial within the shielded frame. For the crew, this entails no proper acceleration—propulsion arises solely from internal proper-time modulation.

*Single Frame Formulation.* When $u = u_{\mathrm{t,net}}$, the system and field move as a unified entity (FIG. 13):

$$U = m_i c^2 = \gamma_s mc^2 \left(1 - \frac{u^2}{n_s^2 c^2}\right) = mc^2 \sqrt{1 - \frac{u^2}{n_s^2 c^2}}. \tag{257}$$

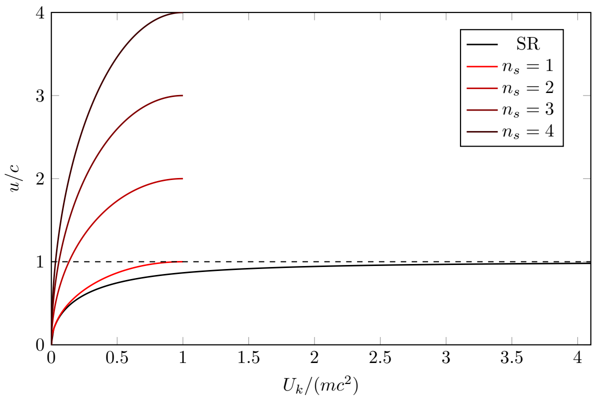


FIG. 14. **Relativistic Velocity.** In special relativity, velocity asymptotically approaches $c$. In inertial shielding, velocity remains bounded by $u = n_s c$.

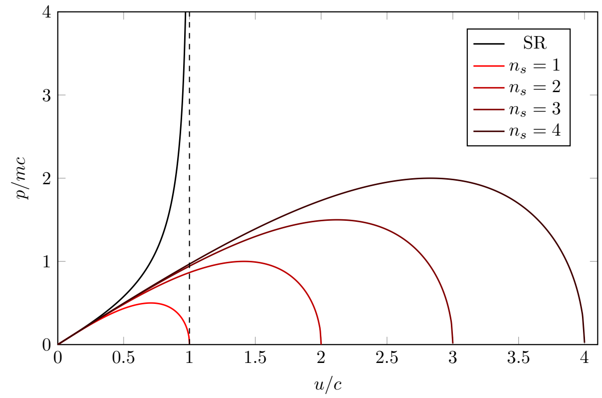


FIG. 15. **Relativistic Momentum.** In special relativity, momentum diverges as $u \to c$. In inertial shielding, momentum remains bounded by $p = mu\sqrt{1 - u^2/(n_s^2 c^2)}$.

For $n_s = 1$, this matches Carezani's Autodynamics [8]:

$$U = m_i c^2 = mc^2 \sqrt{1 - \frac{u^2}{c^2}}. \tag{258}$$

While Carezani did not invoke shielding, the outcome coincides with $u = u_{\text{t,net}}$, where the inertial frame matches the wave field.

Eq. (257) reveals a striking result: as $u \to n_s c$, energy vanishes rather than diverging. The system enters a zero-inertia regime—suggesting physical transparency. This reframes energy, motion, and proper time under internal propulsion, opening pathways beyond conventional relativistic limits.

*Mathematical Verification.* An alternative verification of inertial relativity arises from a physics-mathematics approach, combining physical intuition with formal derivation.

Consider a thought experiment: the inertia of a structure (e.g., a spaceship) is governed by its electromagnetic mass $m = m_{\text{EM}}$, modulated by a factor $n_s^2$ quantifying how many times the rest energy has been confined within a standing wave structure. Once driven by internal forces—specifically momentum transfer from the wave to the structure—the increase in kinetic energy equals the energy extracted from the field:

$$\mathrm{d}U = c^2\,\mathrm{d}m = -\mathrm{d}U_k, \tag{259}$$

$$c^2 \int_m^{m_i} \mathrm{d}m = -\int_0^{u_0} mu'\,\mathrm{d}u', \tag{260}$$

$$m_i c^2 - mc^2 = -\frac{1}{2} m u_0^2. \tag{261}$$

Multiplying by $n_s^2$ and setting $u = n_s u_0$:

$$m_i c^2 = mc^2 \left(1 - \frac{u^2}{2c^2 n_s^2}\right). \tag{262}$$

Postulating $F(u) = \sqrt{1 - f(u)^2}$ with $f(u) = \beta_s = u/n_s c$, we expand:

$$\begin{aligned} F(u) &= \sum_{n=0}^{\infty} \frac{(2n)!}{4^n (n!)^2 (1-2n)} \beta_s^{2n} \\ &= 1 - \frac{1}{2}\beta_s^2 + R(u). \end{aligned} \tag{263}$$

Thus:

$$m_i c^2 = mc^2 \sqrt{1 - \beta_s^2}, \tag{264}$$

$$= mc^2 \left(1 - \frac{u^2}{2n_s^2 c^2} + R(u)\right), \tag{265}$$

with $u \ll c \Rightarrow R(u) \to 0$, recovering Eq. (262).

*Relativistic Energy.* The previous result confirms Eq. (257) and extends it (see FIG. 13) as follows:

$$U = m_i c^2 = mc \left(1 - \frac{u^2}{n_s^2 c^2}\right)^{-1/2} \cdot \left(\frac{dx}{d\tau}\right)_{\text{light}}, \tag{266}$$

$$\left(\frac{dx}{d\tau}\right)_{\text{light}} = c \left(1 - \frac{u_{\text{t,net}}^2}{n_s^2 c^2}\right). \tag{267}$$

For external propulsion ($u_{\text{t,net}} = 0$), inertial shielding becomes inactive, and Einstein's original relativistic energy expression is recovered:

$$n_s = 1 \Rightarrow U = m_i c^2 = mc^2 \left(1 - \frac{u^2}{c^2}\right)^{-1/2}, \tag{268}$$

$$\left(\frac{dx}{d\tau}\right)_{\text{light}} = c. \tag{269}$$

*Velocity from Kinetic Energy.* In special relativity:

$$U_k = m_i c^2 - mc^2 = mc^2 \left(\frac{1}{\sqrt{1 - \frac{u^2}{c^2}}} - 1\right), \tag{270}$$

$$u = c\sqrt{1 - \left(\frac{1}{1 + \frac{U_k}{mc^2}}\right)^2}. \tag{271}$$

*Momentum.* In special relativity:

$$p = m_i u = \frac{mu}{\sqrt{1 - \frac{u^2}{c^2}}}. \tag{272}$$

*Inertial Relativity Formulation.* For $u = u_{\mathrm{t,net}}$, we obtain (see FIG. 13):

$$U = m_i c^2 = mc^2 \sqrt{1 - \frac{u^2}{n_s^2 c^2}}. \tag{273}$$

Kinetic energy (FIG. 14):

$$U_k = mc^2 \left(1 - \sqrt{1 - \frac{u^2}{n_s^2 c^2}}\right), \tag{274}$$

$$u = n_s c \sqrt{1 - \left(1 - \frac{U_k}{mc^2}\right)^2}. \tag{275}$$

Momentum (FIG. 15):

$$p = mu \sqrt{1 - \frac{u^2}{n_s^2 c^2}}. \tag{276}$$

*Engineering Calculations.* Constructing an inertial warp drive remains a formidable challenge. Based on the preceding analysis, we present preliminary estimates—covering energy density, operating frequency, maximum velocity, and candidate materials. While light-speed travel may be decades away, low-speed prototypes below the sonic threshold could be feasible within a few years.

Early concepts turned to superconductors, seeking to harness the Meissner effect. Yet conventional materials impose severe constraints: low critical fields ($\sim 0.1$ T) and isotropic expulsion that risks internal penetration. The path forward points to alternatives capable of withstanding fields beyond 100 T, operating free of cryogenic burdens, and offering directional control.

A more intriguing avenue explores electromagnetic ground waves—familiar from LW and MW bands—engineered to form counter-propagating surface standing waves along a spherical shell. Such waves cling to the surface, slightly penetrating the metallic body, suggesting a mechanism for confinement and controlled interaction that conventional superconductors cannot achieve.

In all cases, the field must remain outside the shell. This allows phase modulation to accelerate confined energy density and generate an inertial field that shields the spaceship from directional acceleration, ensuring no proper force is felt by the crew.

Assuming surface-bound standing waves can be precisely controlled (FIG. 16), and adopting $u = 10c$, $R = 100$ m, and $u_g \approx c$, we select the wavelength such that each hemisphere supports half a guided wave:

$$\frac{\lambda_g}{2} = 2\pi R \approx 628\,\mathrm{m}, \tag{277}$$

$$f = \frac{c}{\lambda_g} \approx 238.8\,\mathrm{kHz} \Rightarrow T = 1/f \approx 4.18 \cdot 10^{-6}\,\mathrm{s}. \tag{278}$$

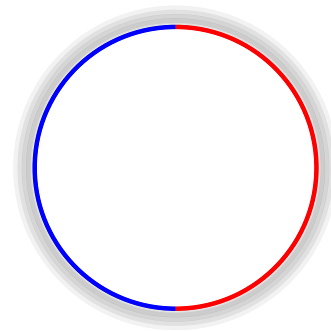

FIG. 16. **Inertial Shielding.** The inertial field (gray) envelops the interior, shielding it from acceleration. Ideally, the energy density should reside outside the shell, confined strictly to its curvature. The blue shell represents a clockwise (CW) accelerating standing wave, while the red shell corresponds to a counterclockwise (CCW) accelerating standing wave.

This ensures wavefronts are phase-locked to the shell curvature, enabling directional acceleration and inertial field generation.

*Superluminal Velocity and Energy Requirements.* To achieve $u = 10c$ with $\Delta\phi = \pi$, the inertial field energy density is (corresponds to a single standing wave):

$$w_{\mathrm{EM}} = \frac{D_G^2}{\varepsilon_{g_0}} = c^2 \mu_{i_0} D_I^2 \approx 1.073 \cdot 10^{28}\,\mathrm{J/m^3}, \tag{279}$$

$$E \approx \sqrt{w_{\mathrm{EM}}/\varepsilon_0} \approx 3.48 \cdot 10^{19}\,\mathrm{V/m}, \tag{280}$$

$$a_{\mathrm{EM}} = D_G = D_I = 3 \cdot 10^9\,\mathrm{m/s^2}. \tag{281}$$

For shell thickness $\delta = 1$ m and radius $R = 100$ m:

$$V_{\mathrm{EM}} = \frac{4\pi}{3}\left[(R+\delta)^3 - R^3\right] \approx 4\pi R^2 \delta \approx 1.2692 \cdot 10^5\,\mathrm{m^3},$$

$$A_{\partial V} \approx 2\pi(R + \delta/2) \cdot 2\pi(\delta/2) \approx 1.98 \cdot 10^3\,\mathrm{m^2},$$

$$U_s = U_{\mathrm{EM}} = V_{\mathrm{EM}} \cdot w_{\mathrm{EM}} \approx 1.3619 \cdot 10^{33}\,\mathrm{J}, \tag{282}$$

$$m_{\mathrm{EM}} = A_{\partial V} \cdot E \sqrt{\varepsilon_0/\varepsilon_{g_0}} \approx 7.095 \cdot 10^{21}\,\mathrm{kg}. \tag{283}$$

Assuming wave cycle duration $T = 1/f \approx 4.19 \cdot 10^{-6}$ s, total energy (net centripetal plus net tangential):

$$U_{\mathrm{total}} \approx 4 \cdot U_{\mathrm{EM}} \approx 5.4476 \cdot 10^{33}\,\mathrm{J}. \tag{284}$$

With coupling efficiency $\kappa_m \approx 0.01$:

$$U_{\mathrm{eff}} \approx \frac{U_{\mathrm{total}}}{\kappa_m} \approx 5.4476 \cdot 10^{35}\,\mathrm{J}. \tag{285}$$

*Relativistic vs Electromagnetic Energy.* Earlier, we set $m = m_{\mathrm{EM}}$ to derive a new relativistic expression with notation parallel to special relativity. This formulation extends the relativistic framework, reducing special relativity to a special case applicable only to propulsion by external forces.

Furthermore, the extension of relativity applies not to the bare inertial mass but to an electromagnetic inertia. As noted in our brief description of magneto-polaritons, when excitations such as dipoles interact with a magnetic field, the bulk material acquires a rest energy related to its electromagnetic mass in the excited state.

By analogy, a spaceship shell interacting with the electromagnetic field acquires an effective electromagnetic inertia, which can be controlled through the same electromagnetic mechanisms.

This implies that Einstein's energy relation $mc^2$, which describes the annihilation of rest mass into equivalent energy, does not apply to electromagnetic mass. Instead, we have

$$mc^2 \neq m_{\mathrm{EM}}c^2 \neq V_{\mathrm{EM}} \cdot w_{\mathrm{EM}} = \frac{V_{\mathrm{EM}} \cdot a_{\mathrm{EM}}^2}{\varepsilon_{g_0}}. \tag{286}$$

*Reconciling Alcubierre Energy with Inertial Shell Dynamics.* Starting from:

$$U_{\mathrm{A}} \approx \frac{c^2}{G} \cdot \frac{v^2 R^2}{\delta}, \tag{287}$$

we multiply and divide by $4\pi$ and $T^2$:

$$U_{\mathrm{A}} \approx 4\pi R^2 \cdot \frac{(cT)^2}{\delta} \cdot \left(\frac{v}{T}\right)^2 \cdot \frac{1}{4\pi G}, \tag{288}$$

$$\approx 4\pi R^2 \cdot \frac{(cT)^2}{\delta} \cdot \frac{a_{\mathrm{EM}}^2}{\varepsilon_{g_0}}, \tag{289}$$

$$v = \omega \cdot R \Rightarrow \frac{v}{T} = a_{\mathrm{EM}}. \tag{290}$$

Defining:

$$V_{\mathrm{A}} = 4\pi R^2 \cdot (cT)^2/\delta, \tag{291}$$

$$w_{\mathrm{EM}} = a_{\mathrm{EM}}^2/\varepsilon_{g_0}, \tag{292}$$

we recover:

$$U_{\mathrm{A}} \approx V_{\mathrm{A}} \cdot w_{\mathrm{EM}}. \tag{293}$$

Setting $\delta = cT$:

$$V_{\mathrm{A}} \approx 4\pi R^2 \delta \approx V_{\mathrm{EM}} \quad \Rightarrow \quad U_{\mathrm{A}} \approx U_{\mathrm{EM}}, \tag{294}$$

establishing structural equivalence between Alcubierre warp energy and inertial shell energy for a single standing wave.

The substitution $\delta = cT$ converts the Alcubierre bubble's associated energy volume into an electromagnetic volume, implying that the bubble behaves as an inertial shell. This bridges spacetime-curvature engineering with classical field-based propulsion and allows warp energy to be reformulated without exotic matter.

*Velocity Acquisition and Modulation.* A key unresolved issue is how the spaceship sustains velocity beyond phase modulation tailored to acceleration. At constant velocity, inertial shielding for both propulsion and the inner shell (crew) deactivates, since it functions only during acceleration. This implies that separate shielding for propulsion and the inner shell should be applied.

The calculated equivalent electric field strength in this configuration is approximately 26 times the Schwinger limit $E_{\mathrm{S}} = \frac{m_e^2 c^3}{e\hbar} \approx 1.32 \cdot 10^{18}\,\mathrm{V/m}$, suggesting a safe acceleration bound $\approx 1.14 \cdot 10^8\,\mathrm{m/s^2}$ corresponding to $\approx 1.54 \cdot 10^{25}\,\mathrm{J/m^3}$.

## XIII. CONCLUSION

This work reexamines the longstanding dismissive treatment of inertial propulsion, reframing it not as a violation of Newtonian mechanics but as a misapplication of its assumptions. By analyzing systems with cyclic, non-collinear internal dynamics, we show that self-contained momentum exchange can yield net translation of an isolated system without violating conservation laws. This resolves the inertial drive paradox and provides a coherent basis for decades of anomalous experimental reports. We developed a continuum of propulsion architectures, from counter-orbiting masses to accelerating standing waves confined within mechanical and electromagnetic structures. These analogs demonstrate how phase modulation and tangential acceleration can produce thrust and inertial shielding, while mistuned configurations may lead to bound motion. Crucially, we introduced a formal coupling between electromagnetism, inertia, and gravity via the energy density expression, offering a unified framework for interpreting gravitational shielding and electromagnetic thrust. Building on this foundation, we derived a relativistic extension—termed *inertial relativity*—which incorporates proper-time modulation and inertial scaling. This framework supports continuous acceleration across the light-speed threshold without invoking exotic matter or spacetime curvature. Benchmarking against the Alcubierre metric shows orders-of-magnitude lower energy requirements, suggesting warp-like motion may be achievable through engineered modulation of inertial response rather than spacetime distortion. Together, these results establish a physically consistent and testable foundation for self-contained propulsion. They invite a reexamination of past anomalies, a redefinition of inertial mass as a dynamic electromagnetic quantity, and the development of a new class of propulsion systems operating without reaction mass. If validated, this framework could mark a turning point in propulsion science—expanding mechanics and enabling spacecraft to traverse space with unprecedented efficiency and velocities beyond conventional limits.

[1] I. Newton, *Philosophiæ Naturalis Principia Mathematica*, Royal Society, 1687.
[2] A. Einstein, *On the Electrodynamics of Moving Bodies*, Annalen der Physik, 1905.
[3] A. Einstein, *The Field Equations of Gravitation*, Akademie der Wissenschaften zu Berlin, 1915.
[4] N. L. Dean, *System for Converting Rotary Motion into Unidirectional Motion*, 1959.
[5] V. N. Tolchin, *Inertoid. Forces of Inertia as a Source of Forward Motion*, Perm Book Publishing, 1977.
[6] E. Podkletnov and R. Nieminen, *A possibility of gravitational force shielding by bulk YBaCuO superconductor*, Physica C, 1992, 10.1016/0921-4534(92)90055-H.
[7] M. Alcubierre, *The warp drive: hyper-fast travel within general relativity*, Classical and Quantum Gravity, 1994, 10.1088/0264-9381/11/5/001.
[8] R. L. Carezani, *Autodynamics: Fundamental Basis for a New Relativistic Mechanics*, SAA Publications, 1998. ISBN 978-0966553307.
[9] S. G. Dimitriou, *On the pendulum oscillations of a suspended RF resonant circuit*, Propulsion Conference, Nevada, 1999.
[10] F. De Aquino, *Possibility of Control of the Gravitational Mass by Means of Extra-Low Frequencies Radiation*, arXiv, 2000, abs/gr-qc/0005107.
[11] J. Wisdom, *Swimming in Spacetime: Motion by Cyclic Changes in Body Shape*, Science, 2003, 10.1126/science.1081406
[12] B. V. Ivanov, *Strong Gravitational Force Induced by Static Electromagnetic Fields*, 2004, gr-qc/0407048
[13] Y. N. Ivanov, *Rhythmodynamics*, 2nd Edition, Energia Publishing, 2007. ISBN 978-5-98420-018-9.
[14] I. A. Loukanov and S. Stoyanov, *Design and Construction of a Gyroscopic Propulsion Mechanism*, 2019, docs/cp19/bp.
[15] A. Geröcs, G. R. Gillich, D. Nedelcu, and Z. I. Korka, *A Multibody Inertial Propulsion Drive with Symmetrically Placed Balls Rotating on Eccentric Trajectories*, Symmetry, 2020, 10.3390/sym12091422.
[16] J. F. Woodward, *Keeping the Dream Alive: Is Propellantless Propulsion Possible?*, IntechOpen, 2021, 10.5772/intechopen.95603.
[17] H. White, P. March, J. Lawrence, J. Butler, S. Mercer, A. Briggs, and P. Meadows, *Measurement of Impulsive Thrust from a Closed Radio Frequency Cavity in Vacuum*, Journal of Propulsion and Power, 2016.
[18] M. Tajmar and G. Fiedler, *Direct Thrust Measurements of an EM Drive and Evaluation of Possible Side-Effects*, AIAA Joint Propulsion Conference, 2015, 10.2514/6.2015-4083.
[19] R. Shawyer, *EM Drive - Advances in Spacecraft Thrusters and Propulsion Systems*, CRC Press, 2023, 10.1201/9781003456759.
[20] C. G. Provatidis, *Inertial Propulsion Devices: A Review*, Eng, 2024, 10.3390/eng5020046.
[21] M. Tajmar, M. Kößling, and O. Neunzig, *In-depth experimental search for a coupling between gravity and electromagnetism with steady fields*, Scientific Reports, 2024, 10.1038/s41598-024-70286-w.
[22] I. Xydous, *Hidden Geometries in Maxwell's Equations and a Force–Flux Route to Unified Static Fields*, Zenodo, September 2025, 10.5281/zenodo.17175682.